Mori–Tanaka estimates of the effective elastic properties of stress-gradient composites

V.P. Tran[a,b], S. Brisard[a,*], J. Guilleminot[c], K. Sab[a]

[a] *Université Paris-Est, Laboratoire Navier, ENPC, IFSTTAR, CNRS UMR 8205, 6 et 8 avenue Blaise Pascal, 77455 Marne-la-Vallée Cedex 2, France*
[b] *Université Paris-Est, Laboratoire Modélisation et Simulation Multi Échelle (MSME UMR 8208 CNRS), 5 boulevard Descartes, Champs-sur-Marne, 77454 Marne-la-Vallée, France*
[c] *Department of Civil and Environmental Engineering, Duke University, Durham, NC 27708, USA*

Abstract

A stress-gradient material model was recently proposed by Forest and Sab [*Mech. Res. Comm.* **40**, 16–25, 2012] as an alternative to the well-known strain-gradient model introduced in the mid 60s. We propose a theoretical framework for the homogenization of stress-gradient materials. We derive suitable boundary conditions ensuring that Hill–Mandel's lemma holds. As a first result, we show that stress-gradient materials exhibit a softening size-effect (to be defined more precisely in this paper), while strain-gradient materials exhibit a stiffening size-effect. This demonstrates that the stress-gradient and strain-gradient models are not equivalent as intuition would have it, but rather complementary. Using the solution to Eshelby's spherical inhomogeneity problem that we derive in this paper, we propose Mori–Tanaka estimates of the effective properties of stress-gradient composites with spherical inclusions, thus opening the way to more advanced multi-scale analyses of stress-gradient materials.

Keywords: Boundary Conditions, Elasticity, Homogenization, Inhomogeneity, Micromechanics, Stress-gradient

1. Introduction

Due to its lack of material internal length, classical elasticity fails to account for size effects frequently exhibited by e.g. nanomaterials. Generalized continua, which were introduced throughout the 20th century have the ability to overcome this shortcoming. The literature on generalized continua is very rich, and we only point at the most salient features of some models, in order to contrast them with the newly introduced stress-gradient model (Forest and Sab, 2012; Sab et al., 2016). The interested reader should refer to e.g. Askes and Aifantis (2011) for a more thorough overview. Higher-order and higher-grade models (to be discussed below) on the one hand share the same underlying idea: their strain energy mixes two or more strain variables which are not dimensionally homogeneous, effectively introducing material parameters that must be homogeneous to their ratio. Non-local models, on the other hand, assume that the local stress at a material point is related to the strains in a neighborhood of this material point (Eringen, 2002); clearly, the *size* of this neighborhood then defines a material internal length.

The Cosserat model (Cosserat and Cosserat, 1909) is probably the earliest example of generalized continua. It belongs to the class of higher-order continua, where additional degrees of freedom (namely, rotations) that account for some underlying microstructure are introduced at each material point. Elastic-plastic extensions of this model have been successfully used to explain the formation of finite-width shear bands in granular media (Mühlhaus and Vardoulakis, 1987). Other examples of higher-order continua are the so-called micromorphic, microstretch and micropolar materials (Eringen, 1999).

The strain-gradient model was introduced by Mindlin (1964) [and recently revisited by Broese et al. (2016)] as the long wavelength approximation of a more general material model for which a micro-volume is attached to any material point (Mindlin, 1964); it is the most simple example of higher-grade continua, in which the elastic strain energy depends on the strain and its first gradient. Mindlin discussed three equivalent forms of this theory (Mindlin and Eshel, 1968); he later introduced second gradient models in order to account for cohesive forces and surface tensions (Mindlin, 1965). The general first-gradient model requires in the case of isotropic, linear elasticity five additional material constants besides the two classical Lamé coefficients (Mindlin and Eshel, 1968) [this was recently questioned by Zhou et al. (2016), who introduced a subclass of isotropic materials for which only three additional material constants are needed]. Identification of strain-gradient material models can therefore be a daunting task, and Altan and Aifantis (1992, 1997) intro-

*Corresponding author.
Email addresses: vinh-phuc.tran@enpc.fr (V.P. Tran), sebastien.brisard@ifsttar.fr (S. Brisard), johann.guilleminot@duke.edu (J. Guilleminot), karam.sab@enpc.fr (K. Sab)

duced a simplified model requiring only one material internal length. This model was later refined by Gao and Park (2007), who clarified the associated boundary conditions.

Having in mind the work of Mindlin and others on strain-gradient materials, it is natural to follow the path towards stress-gradient materials. While the formulation of strain-gradient models relies on the elastic strain energy depending on the strain and its first-gradient, stress-gradient models rely on the complementary elastic strain energy depending on the stress and its first gradient. From this perspective, the Bresse–Timoshenko beam model (Timoshenko, 1921) can be seen as the first stress-gradient model, since the complementary energy of such beams depends on the bending moment and its derivative [see also (Challamel et al., 2016a)]. Despite this historical precedent, it was several decades before other stress-gradient theories were proposed, for plates (Lebée and Sab, 2011, 2017a,b), then for continua (Forest and Sab, 2012; Polizzotto, 2014). The reason for this relatively large time lapse can probably be attributed to the generally accepted premise that (owing to the linear stress-strain relationship) strain- and stress-gradient models should be equivalent. It is in fact a misconception: as will be shown in the present paper, the two material models are *complementary* rather than *equivalent*.

Due to the existence of at least one material internal length, homogenization of generalized continua produces macroscopic models which exhibit size-effects. In other words, the homogenized stiffness depends (at fixed volume fraction) on the absolute size of the inclusions. Generalized continua therefore appear as interesting ad-hoc microscopic models for materials that exhibit size-effects but behave otherwise classically at the macroscopic scale. Mori–Tanaka estimates of the size-dependent macroscopic stiffness were thus proposed for e.g. the micropolar (Sharma and Dasgupta, 2002), second gradient (Zhang and Sharma, 2005) and simplified strain gradient (Ma and Gao, 2014) theories, successively. In all instances, the macroscopic stiffness was found to increase as the size of the inclusions decreased (the material internal lengths being fixed). This effect is usually referred to as the stiffening size-effect.

The goal of this work is the homogenization of stress-gradient materials. To this end, we set up a framework based on a generalized Hill–Mandel's lemma, from which we derive boundary conditions that are suitable to the computation of the apparent compliance of linearly elastic materials. In particular, we show that contrary to strain-gradient materials, stress-gradient materials exhibit a softening size-effect. We then set out to compute micromechanical estimates of the effective compliance of isotropic, linear elastic materials. We show that, in general, such materials are defined by three material internal lengths. Drawing inspiration from the works of Altan and Aifantis (1992, 1997) and Gao and Park (2007), we propose a so-called *simplified* stress-gradient model with only one material internal length. We then solve Eshelby's spherical inhomogeneity problem for this simplified model. Finally, the resulting analytical solution is implemented in a Mori–Tanaka scheme. This estimate is compared with that obtained by Ma and Gao (2014) for strain-gradient elasticity.

The paper is organized as follows. Section 2 recalls the derivation of the stress-gradient model introduced by Forest and Sab (2012) and Sab et al. (2016). Only the essential steps of the derivation are recalled (the reader being referred to the above cited references for detailed calculations and proofs). Section 3 then discusses linear, stress-gradient elasticity and introduces our simplified model. Section 4 addresses homogenization of stress-gradient materials (in the case of microscopic material internal lengths). Eshelby's spherical inhomogeneity problem is then solved in section 5. The derivation is quite lengthy, and is only sketched out. Finally, section 6 is devoted to the implementation of the Mori–Tanaka scheme for stress-gradient materials.

In the remainder of this paper, we will deal with second-, third-, fourth- and sixth-rank tensors. In most situations, the rank of the tensor can be inferred from the context: therefore, the same typeface (namely, bold face) will be adopted for all tensors, regardless of their rank. However, where confusion can occur, the rank of the tensor under consideration will be specified with a lower-right index, e.g. $\mathbf{T}_3$, rather than $\mathbf{T}$. We then define the following spaces of second-, third-, fourth- and sixth-rank

$$\mathcal{T}_2 = \{\mathbf{T} = T_{ij}\mathbf{e}_i \otimes \mathbf{e}_j, \text{ such that } T_{ij} = T_{ji}\}, \tag{1a}$$
$$\mathcal{T}_3 = \{\mathbf{T} = T_{ijk}\mathbf{e}_i \otimes \mathbf{e}_j \otimes \mathbf{e}_k, \text{ such that } T_{ijk} = T_{jik}\}, \tag{1b}$$
$$\mathcal{T}_4 = \{\mathbf{T} = T_{ijpq}\mathbf{e}_i \otimes \mathbf{e}_j \otimes \mathbf{e}_p \otimes \mathbf{e}_q, \text{ such that } T_{ijpq} = T_{jipq} = T_{ijqp}\}, \tag{1c}$$
$$\mathcal{T}_6 = \{\mathbf{T} = T_{ijkpqr}\mathbf{e}_i \otimes \mathbf{e}_j \otimes \mathbf{e}_k \otimes \mathbf{e}_p \otimes \mathbf{e}_q \otimes \mathbf{e}_r, \text{ such that } T_{ijkpqr} = T_{jikpqr} = T_{ijkqpr}\}. \tag{1d}$$

In other words, $\mathcal{T}_2$ denotes the space of symmetric, second-rank tensors; $\mathcal{T}_4$ denotes the associated space of fourth-rank tensors with minor symmetries. Likewise, $\mathcal{T}_3$ denotes the space of third-rank tensors, symmetric with respect to their first two indices, while the symmetries of the elements of $\mathcal{T}_6$ are consistent with those of the elements of $\mathcal{T}_3$. Unless otherwise stated, all tensors considered in the present paper will be taken in one of the spaces defined above. Therefore, statements like "n-th rank tensor $\mathbf{T}$" will always assume that the tensor $\mathbf{T}$ under consideration is an element of $\mathcal{T}_n$.

This is consistent with the fact that the gradient $\mathbf{T} \otimes \nabla = \partial_i \mathbf{T} \otimes \mathbf{e}_i$ of a second-rank, symmetric tensor $\mathbf{T}$ is symmetric with respect to its first two indices: in other words, if $\mathbf{T} \in \mathcal{T}_2$, then $\mathbf{T} \otimes \nabla \in \mathcal{T}_3$.

The trace of a second-rank tensor is classically defined as its total contraction; similarly, we define the trace of a third-rank tensor as its contraction with respect to its last two indices. The trace of $\mathbf{T} \in \mathcal{T}_3$ is therefore the *vector* $\mathbf{T} : \mathbf{I}_2 = \mathbf{T}_{ijj}\mathbf{e}_i$, and it is observed that the divergence $\mathbf{T} \cdot \nabla$ of a second-rank tensor $\mathbf{T} \in \mathcal{T}_2$ is the trace of its gradient: $\mathbf{T} \cdot \nabla = (\mathbf{T} \otimes \nabla) : \mathbf{I}_2$. It will be convenient to introduce the space $\mathcal{T}_3' \subset \mathcal{T}_3$ of third-rank, trace-free tensors

$$\mathcal{T}_3' = \{\mathbf{T} \in \mathcal{T}_3, \mathbf{T} : \mathbf{I}_2 = \mathbf{0}\}. \tag{2}$$

To close this section, we recall the components of the iden-

tity tensors $\mathbf{I}_2 \in \mathcal{T}_2, \mathbf{I}_4 \in \mathcal{T}_4$ and $\mathbf{I}_6 \in \mathcal{T}_6$

$$\mathbf{I}_2 = \delta_{ij}\, \mathbf{e}_i \otimes \mathbf{e}_j, \tag{3a}$$
$$\mathbf{I}_4 = \tfrac{1}{2}(\delta_{ip}\delta_{jq} + \delta_{iq}\delta_{jp})\mathbf{e}_i \otimes \mathbf{e}_j \otimes \mathbf{e}_p \otimes \mathbf{e}_q, \tag{3b}$$
$$\mathbf{I}_6 = I_{ijpq}\, \delta_{kr}\, \mathbf{e}_i \otimes \mathbf{e}_j \otimes \mathbf{e}_k \otimes \mathbf{e}_p \otimes \mathbf{e}_q \otimes \mathbf{e}_r. \tag{3c}$$

2. The stress-gradient model

In the present section, we give a brief overview of the elastic stress-gradient model introduced by Forest and Sab (2012). The basic assumptions of the model are first stated in section 2.1. The equations of the elastic equilibrium of stress-gradient materials are then recalled in section 2.2. It should be emphasized that the results presented here are not new: they were first introduced by Forest and Sab (2012); it was later shown by Sab et al. (2016) that the model was mathematically sound, to the point that it was successfully extended to finite-deformation (Forest and Sab, 2017).

2.1. General assumptions of the model

In classical elasticity, the complementary stress energy of a Cauchy material occupying the domain $\Omega \subset \mathbb{R}^3$ is given by the following general expression

$$W^*(\boldsymbol{\sigma}) = \int_{\mathbf{x}\in\Omega} w^*(\mathbf{x}, \boldsymbol{\sigma}(\mathbf{x}))\, \mathrm{d}V_{\mathbf{x}}, \tag{4}$$

where w^* denotes the volume density of complementary strain energy. It depends explicitly on the observation point $\mathbf{x} \in \Omega$ to account for material heterogeneities.

In the model of Forest and Sab (2012), stress-gradient materials are defined as continua for which the *Stress Principle of Cauchy* still applies (Marsden and Hughes, 1994, §2.2), while the complementary stress energy density now depends on the local stress *and* its first gradient

$$\begin{aligned} W^*(\boldsymbol{\sigma}) &= \int_{\mathbf{x}\in\Omega} w^*(\mathbf{x}, \boldsymbol{\sigma}(\mathbf{x}), \boldsymbol{\sigma}\otimes\nabla(\mathbf{x}))\, \mathrm{d}V_{\mathbf{x}} \\ &= \int_{\Omega} w^*(\boldsymbol{\sigma}, \boldsymbol{\sigma}\otimes\nabla)\, \mathrm{d}V, \end{aligned} \tag{5}$$

where the explicit dependency on the observation point $\mathbf{x} \in \Omega$ has been omitted.

It is emphasized that the equilibrium of stress-gradient materials thus defined remains governed by the classical principles (in other words, the definition of statically admissible stress fields is unchanged). In particular, the traction $\boldsymbol{\sigma}\cdot\mathbf{n}$ must be continuous accross any discontinuity surface ($\mathbf{n}$: normal to the surface). We will write $[\![\boldsymbol{\sigma}]\!]\cdot\mathbf{n} = \mathbf{0}$, where $[\![\bullet]\!]$ denotes the jump across the surface. Traction continuity is a minimum regularity requirement, resulting from the Stress Principle of Cauchy. We will see in section 2.2 that the higher-order constitutive law of stress-gradient materials in fact requires continuity of the *full* Cauchy stress tensor $\boldsymbol{\sigma}$.

It results from the equilibrium equation $\boldsymbol{\sigma}\cdot\nabla + \mathbf{b} = \mathbf{0}$ ($\mathbf{b}$: volume density of body forces) that all components of the stress-gradient $\boldsymbol{\sigma}\otimes\nabla$ do not play equal roles. Indeed, its trace (as defined in section 1) is constrained

$$(\boldsymbol{\sigma}\otimes\nabla) : \mathbf{I}_2 = (\boldsymbol{\sigma}\cdot\nabla) = -\mathbf{b}, \tag{6}$$

and optimization of the complementary stress energy (5) must account for this constraint.

This suggests the following decomposition of the stress-gradient tensor as the sum of two third-rank tensors: $\boldsymbol{\sigma}\otimes\nabla = \mathbf{Q} + \mathbf{R}$, where $\mathbf{R} \in \mathcal{T}_3'$ is trace-free ($\mathbf{R} : \mathbf{I}_2 = \mathbf{0}$).

Under the additional orthogonality condition $\mathbf{R} \therefore \mathbf{Q} = R_{ijk}Q_{ijk} = 0$ (where "$\therefore$" denotes the contraction over the last three indices of the left operand and the first three indices of the right operand), it was shown by Forest and Sab (2012) that this decomposition was unique [see also Sab et al. (2016), as well as Appendix A of the present paper]. These authors called $\mathbf{R}$ (resp. $\mathbf{Q}$) the *deviatoric* (resp. *spherical*) part of the stress-gradient $\boldsymbol{\sigma}\otimes\nabla$. In the present paper, we will refrain from using this terminology, as alternative definitions for the deviatoric and spherical parts of third-rank tensors have been proposed in the literature. For example, third-rank tensors are deviatoric in the sense of Monchiet and Bonnet (2010) if their contraction on *any* pair of indices is null. From our perspective, only the contraction on the last two indices is meaningful (as it relates to the connexion between gradient and divergence of a tensor field).

It is convenient to introduce the sixth-rank projection tensor $\mathbf{I}_6'$ such that $\mathbf{R} = \mathbf{I}_6' \therefore (\boldsymbol{\sigma}\otimes\nabla)$. In other words, $\mathbf{I}_6'$ is the orthogonal projector onto the subspace $\mathcal{T}_3'$ of trace-free, third rank tensors; it can be seen as the identity for this subspace. Some properties of $\mathbf{I}_6'$ are gathered in Appendix A. The volume density of complementary strain energy is now viewed as a function of $\boldsymbol{\sigma}$, $\mathbf{R}$ and $\mathbf{Q}$: $w^*(\boldsymbol{\sigma}, \mathbf{R}, \mathbf{Q})$. However, the third argument of w^* is fixed, since $\mathbf{Q} = -\frac{1}{2}\mathbf{I}_4\cdot\mathbf{b}$ [see equation (A.5) in Appendix A]. As a consequence, there is no strain measure associated with $\mathbf{Q}$, which plays the role of a prestress.

Forest and Sab (2012) omitted this prestress, as its physical meaning remains unclear. In other words, the complementary strain energy density w^* depends on $\boldsymbol{\sigma}$ and $\mathbf{R}$ only. Equation (5) is then replaced with

$$W^*(\boldsymbol{\sigma}, \mathbf{R}) = \int_{\Omega} w^*(\boldsymbol{\sigma}, \mathbf{R})\, \mathrm{d}V, \quad \text{where} \quad \mathbf{R} = \mathbf{I}_6' \therefore (\boldsymbol{\sigma}\otimes\nabla), \tag{7}$$

which effectively defines the stress-gradient model of Forest and Sab (2012).

2.2. Equilibrium of clamped, elastic, stress-gradient bodies

It was shown by Sab et al. (2016) that minimizing the complementary stress energy W^* defined by equation (7) results in the following boundary-value problem

$$\boldsymbol{\sigma}\cdot\nabla + \mathbf{b} = \mathbf{0} \qquad \mathbf{R} = \mathbf{I}_6' \therefore (\boldsymbol{\sigma}\otimes\nabla), \tag{8a}$$
$$\mathbf{e} = \partial_{\boldsymbol{\sigma}} w^* \qquad \mathbf{I}_6' \therefore \boldsymbol{\psi} = \partial_{\mathbf{R}} w^*, \tag{8b}$$
$$\mathbf{e} = \boldsymbol{\psi}\cdot\nabla, \tag{8c}$$
$$\boldsymbol{\psi}\cdot\mathbf{n}|_{\partial\Omega} = \mathbf{0}, \tag{8d}$$

which effectively defines a *clamped*, stress-gradient body (since the potential of prescribed displacements is null). In the above

boundary-value problem, equations (8a), (8b) and (8c) are field equations (defined over the whole domain Ω), while equation (8d) is a kinematic boundary condition.

The third-rank tensor $\boldsymbol{\psi}$ is the Lagrange multiplier involved in the constrained minimization of the complementary stress energy. More precisely, its trace $\mathbf{u} = \frac{1}{2}\boldsymbol{\psi} : \mathbf{I}_2$ is the Lagrange multiplier associated with the constraint $(8a)_1$ (equilibrium equation), while its trace-free part $\boldsymbol{\phi} = \mathbf{I}'_6 \therefore \boldsymbol{\psi}$ is the Lagrange multiplier associated with $(8a)_2$. It plays the role of *both* a generalized strain [see equation $(8b)_2$] and a generalized displacement [see equations $(8b)_1$ and (8c)], and we have [see equation (A.4) in Appendix A]

$$\boldsymbol{\psi} = \boldsymbol{\phi} + \mathbf{I}_4 \cdot \mathbf{u}, \quad \mathbf{u} = \tfrac{1}{2}\boldsymbol{\psi} : \mathbf{I}_2 \quad \text{and} \quad \boldsymbol{\phi} = \mathbf{I}'_6 \therefore \boldsymbol{\psi}. \tag{9}$$

The strain measure $\mathbf{e}$ that is energy-conjugate to the stress $\boldsymbol{\sigma}$ [see equation $(8b)_1$] is *not* necessarily the symmetric gradient of a displacement. Indeed, combining equations (8c) and (9)

$$\mathbf{e} = \boldsymbol{\psi} \cdot \nabla = \boldsymbol{\phi} \cdot \nabla + (\mathbf{I}_4 \cdot \mathbf{u}) \cdot \nabla = \boldsymbol{\phi} \cdot \nabla + \boldsymbol{\epsilon}[\mathbf{u}]. \tag{10}$$

To emphasize this unusual point, $\mathbf{e}$ will be called in the remainder of this paper the *total strain*.

The mathematical analysis of problem (8) was recently carried out by Sab et al. (2016). In the case of linear elasticity, assuming uniform ellipticity, these authors showed that problem (8) is well-posed. Besides, across any discontinuity surface, the flux of $\boldsymbol{\psi}$ and the *full* stress tensor $\boldsymbol{\sigma}$ are continuous

$$[\![\boldsymbol{\psi} \cdot \mathbf{n}]\!] = [\![\boldsymbol{\phi} \cdot \mathbf{n} + \mathbf{sym}(\mathbf{u} \otimes \mathbf{n})]\!] = \mathbf{0} \quad \text{and} \quad [\![\boldsymbol{\sigma}]\!] = \mathbf{0}. \tag{11}$$

The last point is rather unusual. It is emphasized that it is a mere result of the modelling assumption that the complementary stress energy should depend on the stress tensor *and* the trace-free part of its gradient [see equation (7)].

As a consequence of this regularity result, it is perfectly acceptable to prescribe the *full* stress tensor at the boundary $\partial\Omega$ of stress-gradient materials. In other words, replacing boundary conditions (8d) with

$$\boldsymbol{\sigma}|_\Omega = \overline{\boldsymbol{\sigma}}, \tag{12}$$

where $\overline{\boldsymbol{\sigma}}$ denotes the prescribed stress tensor, defines a well-posed problem (Sab et al., 2016) (up to a rigid body motion). It should be noted that $\overline{\boldsymbol{\sigma}}$ needs not be constant over $\partial\Omega$. Furthermore, both equations (8d) and (12) result in 6 independent scalar boundary conditions.

It can further be shown that the solution to the boundary value problem defined by equations (8a), (8b), (8c) and (12) minimizes the complementary stress enery $W^*(\boldsymbol{\sigma}, \mathbf{R})$ defined by equation (7), under the constraints (8a) and (12).

Before we close this brief overview of the stress-gradient model, it should be noted that it is of course possible to define more general boundary conditions Sab et al. (2016). However, for the sole purpose of homogenization, it will prove sufficient to prescribe the stress tensor at the boundary. We will therefore focus on the boundary-value problem defined by the field equations (8a)–(8c) and the boundary conditions (12).

2.3. Linear stress-gradient elasticity

The general expression of the complementary energy density w^* reads, in the case of linear elasticity

$$w^*(\boldsymbol{\sigma}, \mathbf{R}) = \tfrac{1}{2}\boldsymbol{\sigma} : \mathbf{S} : \boldsymbol{\sigma} + \tfrac{1}{2}\mathbf{R} \therefore \mathbf{M} \therefore \mathbf{R}, \tag{13}$$

where the fourth-rank tensor $\mathbf{S}$ is the classical compliance of the material and the sixth-rank tensor $\mathbf{M}$ is the generalized compliance. Both $\mathbf{S}$ and $\mathbf{M}$ are symmetric (with respect to the double-dot and triple-dot scalar products, respectively). Since $\mathbf{R}$ is trace-free, $\mathbf{M}$ must further satisfy the following identity

$$\mathbf{M} = \mathbf{I}'_6 \therefore \mathbf{M} \therefore \mathbf{I}'_6. \tag{14}$$

As suggested in Forest and Sab (2012), coupling between the stress tensor $\boldsymbol{\sigma}$ and the trace-free part of its gradient $\mathbf{R} = \mathbf{K} \therefore (\boldsymbol{\sigma} \otimes \nabla)$ was discarded in expression (13) of the complementary strain energy density w^*. For centrosymmetric materials, this coupling vanishes rigorously. The constitutive laws (8b) then read

$$\mathbf{e} = \mathbf{S} : \boldsymbol{\sigma} \quad \text{and} \quad \boldsymbol{\phi} = \mathbf{I}'_6 \therefore \boldsymbol{\psi} = \mathbf{M} \therefore \mathbf{R}, \tag{15}$$

which can readily be inverted as follows

$$\boldsymbol{\sigma} = \mathbf{C} : \mathbf{e} \quad \text{and} \quad \mathbf{R} = \mathbf{L} \therefore \boldsymbol{\phi}, \tag{16}$$

where $\mathbf{C} = \mathbf{S}^{-1}$ denotes the classical stiffness, while $\mathbf{L}$ denotes the generalized stiffness. Attention should be paid to the fact that, because of equation (14), the generalized compliance $\mathbf{M}$ is a singular sixth-rank tensor. It is however invertible within the space $\mathcal{T}'_3$ of trace-free, third-rank tensors; in this sense, the generalized stiffness $\mathbf{L}$ is the inverse of the generalized compliance $\mathbf{M}$, and

$$\mathbf{L} \therefore \mathbf{M} = \mathbf{M} \therefore \mathbf{L} = \mathbf{I}'_6. \tag{17}$$

3. A simplified model for isotropic, linear stress-gradient elasticity

The remainder of this paper is restricted to isotropic, linear, elastic stress-gradient materials. Then, it is shown in Appendix B that the compliance tensors $\mathbf{S}$ and $\mathbf{M}$ of isotropic materials are in general defined by five parameters, namely two elastic moduli and three material internal lengths. This leads to an unpractically complex theory (which would be extremely difficult to identify experimentally). We therefore introduce in the present section a simplified model that depends on *three* material parameters only, namely the classical shear modulus μ and Poisson ratio ν, and one material internal length, ℓ.

The derivation of our simplified stress-gradient model draws on the ideas of Altan and Aifantis (1992, 1997), who proposed a three-parameter material model for strain-gradient elasticity, which is a restriction of Mindlin's general framework (Mindlin and Eshel, 1968). In the simplified model of Altan and Aifantis (1992, 1997) [see also Gao and Park (2007) and Forest and Aifantis (2010)], the strain energy density w reads

$$w = \tfrac{1}{2}\lambda\varepsilon_{ii}\varepsilon_{jj} + \mu\varepsilon_{ij}\varepsilon_{ij} + \ell^2\big(\tfrac{1}{2}\lambda\varepsilon_{ii,k}\varepsilon_{jj,k} + \mu\varepsilon_{ij,k}\varepsilon_{ij,k}\big), \tag{18}$$

where λ and μ are the first and second Lamé coefficients, and ℓ is the material internal length. Similarly, we adopt here the following expression of the elastic stress energy density

$$w^* = \frac{1}{2\mu}[\sigma_{ij}\sigma_{ij} - \tfrac{\nu}{1+\nu}\sigma_{ii}\sigma_{jj} + \ell^2(R_{ijk}R_{ijk} - \tfrac{\nu}{1+\nu}R_{iik}R_{jjk})]. \quad (19)$$

It should be noted that a similar model was proposed by Polizzotto (2016). However, in the present case, equation (14) must be enforced, which makes for slightly more complex expressions of the generalized compliance $\mathbf{M}$. In particular, Eringen's equation $\boldsymbol{\sigma} - \ell^2\Delta\boldsymbol{\sigma} = \mathbf{C} : \boldsymbol{\varepsilon}$ (Eringen, 1983; Altan and Aifantis, 1992, 1997) is not retrieved (see also Forest and Aifantis, 2010, for a discussion of this equation). After simple algebra, it is found from comparing equations (13) and (19)

$$\mathbf{S} = \frac{1}{2\mu}\Big(\tfrac{1-2\nu}{1+\nu}\mathbf{J}_4 + \mathbf{K}_4\Big) \quad \text{and} \quad \mathbf{M} = \frac{\ell^2}{2\mu}\Big(\tfrac{1-2\nu}{1+\nu}\mathbf{J}_6 + \mathbf{K}_6\Big), \quad (20)$$

where $\mathbf{J}_4 = \frac{1}{3}\mathbf{I}_2 \otimes \mathbf{I}_2$ and $\mathbf{K}_4 = \mathbf{I}_4 - \mathbf{J}_4$ are the classical, fourth-rank spherical and deviatoric projection tensors. The sixth-rank projection tensors $\mathbf{J}_6$ and $\mathbf{K}_6$ are defined in Appendix B. The expression of the generalized stiffness $\mathbf{L}$ readily results from the multiplication table B.1

$$\mathbf{C} = 2\mu\Big(\tfrac{1+\nu}{1-2\nu}\mathbf{J}_4 + \mathbf{K}_4\Big) \quad \text{and} \quad \mathbf{L} = \frac{2\mu}{\ell^2}\Big(\tfrac{1+\nu}{1-2\nu}\mathbf{J}_6 + \mathbf{K}_6\Big). \quad (21)$$

Remark 1. *Classical Cauchy elasticity is retrieved for $\ell \to 0$ [see expression (19)].*

Remark 2. *Conversely, for the complementary energy density w^* (18) to remain finite, the trace-free part $\mathbf{R}$ of the stress-gradient $\boldsymbol{\sigma} \otimes \nabla$ must vanish when $\ell \to +\infty$. Furthermore, in the absence of body-forces, $\boldsymbol{\sigma} \cdot \nabla = \mathbf{0}$, and we find that the full stress-gradient vanishes. In other words, the stress field tends to be phase-wise constant when the material internal length becomes large.*

4. Homogenization of heterogeneous, stress-gradient materials

In this section, we consider a heterogeneous body $\mathcal{B}$ composed of stress-gradient materials. Similarly to Cauchy materials, we introduce three different length-scales

1. the typical size d of the heterogeneities,
2. the size L_{meso} of the representative volume element (RVE), the existence of which is postulated,
3. the typical size L_{macro} of the structure and the length scale of its loading.

We assume that the heterogeneous material that the body $\mathcal{B}$ is made of is *homogenizable* and seek its effective behavior. This requires that separation of scales prevails. Besides the standard condition

$$d \ll L_{\text{meso}} \ll L_{\text{macro}}, \quad (22)$$

continua with one material internal length ℓ as defined in section 2.3 further require conditions that involve both the size of the heterogeneities and the internal length. This paper is dedicated to materials for which

$$\ell \sim d \quad \text{or} \quad \ell \ll d. \quad (23)$$

What is the expected macroscopic behavior of such heterogeneous materials? The very same question was explored by Forest et al. (2001) in the case of Cosserat media. By means of asymptotic expansions, these authors proved that under assumption (23), the heterogeneous material behaves macroscopically as a standard, linearly elastic material. The same argument would apply here, leading to the same conclusion. The macroscopic behavior of the heterogeneous, stress-gradient material is then characterized by the effective compliance $\mathbf{S}^{\text{eff}}$, which relates the macroscopic strain $\langle\mathbf{e}\rangle$ to the macroscopic stress $\langle\boldsymbol{\sigma}\rangle$ (where quantities between angle brackets denote volume averages over the RVE) through the standard constitutive equation $\langle\mathbf{e}\rangle = \mathbf{S}^{\text{eff}} : \langle\boldsymbol{\sigma}\rangle$, where the macroscopic variables are the average stress $\langle\boldsymbol{\sigma}\rangle$ and the average *total* strain $\langle\mathbf{e}\rangle$ [defined by equation (10)].

Following the terminology introduced by Huet (1990) (see also Ostoja-Starzewski, 2006), the effective compliance is defined in the present work as the limit for large statistical volume elements (SVE) of the *apparent* compliance. It is then essential that the local problem that defines the apparent compliance satisfies the Hill–Mandel lemma. This is discussed in the next section.

4.1. The local problem and the Hill–Mandel lemma

The apparent compliance of the (finite-size) SVE Ω is classically defined from the solution to a local problem which expresses the elastic equilibrium of the stress-gradient, heterogeneous SVE Ω, subjected to no body forces and appropriate boundary conditions that ensure micro-macro energy consistency. These boundary conditions are identified from the Hill–Mandel lemma, extended to stress-gradient materials as follows

$$\langle\boldsymbol{\sigma}^\dagger : \mathbf{e} + (\boldsymbol{\sigma}^\dagger \otimes \nabla) \therefore \boldsymbol{\phi}\rangle = \langle\boldsymbol{\sigma}^\dagger\rangle : \langle\mathbf{e}\rangle, \quad (24)$$

where $\boldsymbol{\sigma}^\dagger \in \mathcal{T}_2$ is a divergence-free stress tensor, while $\mathbf{u}$ and $\boldsymbol{\phi}$ are derived from an arbitrary third-rank tensor $\boldsymbol{\psi} \in \mathcal{T}_3$ through identities (9). In equation (24), the macroscopic term $\langle\boldsymbol{\sigma}^\dagger \otimes \nabla\rangle \therefore \langle\boldsymbol{\phi}\rangle$ has been discarded, because the homogenized stress-gradient material is expected to behave as a Cauchy material (no macroscopic gradient effect). The left-hand side of equation (24) is first transformed into a surface integral. From equations (9)

$$\begin{aligned}
&\boldsymbol{\sigma}^\dagger : \mathbf{e} + (\boldsymbol{\sigma}^\dagger \otimes \nabla) \therefore \boldsymbol{\phi} \\
&\quad = \boldsymbol{\sigma}^\dagger : \boldsymbol{\epsilon}[\mathbf{u}] + \boldsymbol{\sigma}^\dagger : (\boldsymbol{\phi} \cdot \nabla) + (\boldsymbol{\sigma}^\dagger \otimes \nabla) \therefore \boldsymbol{\phi} \\
&\quad = (\mathbf{u} \cdot \boldsymbol{\sigma}^\dagger) \cdot \nabla - \mathbf{u} \cdot (\boldsymbol{\sigma}^\dagger \cdot \nabla) + (\boldsymbol{\sigma}^\dagger : \boldsymbol{\phi}) \cdot \nabla \\
&\quad = (\boldsymbol{\sigma}^\dagger \cdot \mathbf{u} + \boldsymbol{\sigma}^\dagger : \boldsymbol{\phi}) \cdot \nabla = [\boldsymbol{\sigma}^\dagger : (\mathbf{I}_4 \cdot \mathbf{u} + \boldsymbol{\phi})] \cdot \nabla, \\
&\quad = \boldsymbol{\sigma}^\dagger : \boldsymbol{\psi} \cdot \mathbf{n}, \quad (25)
\end{aligned}$$

where the fact that $\boldsymbol{\sigma}^\dagger$ is divergence-free has been used. From the divergence formula, we then have

$$\langle \boldsymbol{\sigma}^\dagger : \mathbf{e} + (\boldsymbol{\sigma}^\dagger \otimes \nabla) \therefore \boldsymbol{\phi} \rangle = \frac{1}{V} \int_{\partial\Omega} \boldsymbol{\sigma}^\dagger : \boldsymbol{\psi} \cdot \mathbf{n} \, \mathrm{d}S, \tag{26}$$

where $\mathbf{n}$ denotes the outer normal to the boundary $\partial\Omega$ of the SVE Ω. Therefore, the Hill–Mandel lemma holds, provided that

$$\frac{1}{V} \int_{\partial\Omega} \boldsymbol{\sigma}^\dagger : \boldsymbol{\psi} \cdot \mathbf{n} \, \mathrm{d}S = \langle \boldsymbol{\sigma}^\dagger \rangle : \langle \mathbf{e} \rangle. \tag{27}$$

Remark 3. *Plugging $\boldsymbol{\sigma}^\dagger = \text{const.}$ into equation (26), we find the following expression of the macroscopic strain $\langle \mathbf{e} \rangle$*

$$\langle \mathbf{e} \rangle = \frac{1}{V} \int_{\partial\Omega} \boldsymbol{\psi} \cdot \mathbf{n} \, \mathrm{d}S, \tag{28}$$

then, using the decomposition (9) of $\boldsymbol{\psi}$

$$\begin{aligned} \langle \mathbf{e} \rangle &= \frac{1}{V} \int_{\partial\Omega} \boldsymbol{\psi} \cdot \mathbf{n} \, \mathrm{d}S = \frac{1}{V} \int_{\partial\Omega} (\boldsymbol{\phi} + \mathbf{I}_4 \cdot \mathbf{u}) \cdot \mathbf{n} \, \mathrm{d}S \\ &= \frac{1}{V} \int_{\partial\Omega} [\boldsymbol{\phi} \cdot \mathbf{n} + \mathbf{sym}(\mathbf{u} \otimes \mathbf{n})] \mathrm{d}S \\ &= \frac{1}{V} \int_{\Omega} \boldsymbol{\epsilon}[\mathbf{u}] \, \mathrm{d}V + \frac{1}{V} \int_{\partial\Omega} \boldsymbol{\phi} \cdot \mathbf{n} \, \mathrm{d}S. \end{aligned} \tag{29}$$

In other words, the macroscopic strain is in general not the volume average of the symmetrized gradient of the "microscopic displacement" $\mathbf{u}$. $\frac{1}{2}\boldsymbol{\psi} : \mathbf{I}_2$. However, in a random setting (assuming that $\boldsymbol{\phi}$ is a statistically homogeneous and ergodic random process), the last term in the above equation vanishes for Ω sufficiently large. In other words, the classical definition of the macroscopic strain is retrieved in that case.

In the remainder of this section, we prove that so-called *uniform stress boundary conditions* ensure that the Hill–Mandel lemma indeed holds. Starting from the right-hand side of equation (26), we now assume that the divergence-free stress-tensor $\boldsymbol{\sigma}^\dagger$ is fully prescribed at the boundary $\partial\Omega$: $\boldsymbol{\sigma}^\dagger|_{\partial\Omega} = \overline{\boldsymbol{\sigma}}$, where $\overline{\boldsymbol{\sigma}} \in \mathcal{T}_2$ is a constant, prescribed stress. It should be again emphasized that such boundary condition is compatible with the stress-gradient model [see discussion in section 2.2, around equation (12)]. Then, from equation (28)

$$\int_{\partial\Omega} \boldsymbol{\sigma}^\dagger : \boldsymbol{\psi} \cdot \mathbf{n} \, \mathrm{d}S = \overline{\boldsymbol{\sigma}} : \int_{\partial\Omega} \boldsymbol{\psi} \cdot \mathbf{n} \, \mathrm{d}S = V \, \overline{\boldsymbol{\sigma}} : \langle \mathbf{e} \rangle, \tag{30}$$

Furthermore, since $\boldsymbol{\sigma}$ is divergence-free, we have classically for all displacement field $\mathbf{u}$

$$\begin{aligned} \langle \boldsymbol{\sigma}^\dagger : \boldsymbol{\epsilon}[\mathbf{u}] \rangle &= \frac{1}{V} \int_{\partial\Omega} \mathbf{u} \cdot \boldsymbol{\sigma}^\dagger \cdot \mathbf{n} \, \mathrm{d}S = \frac{1}{V} \int_{\partial\Omega} \mathbf{u} \cdot \overline{\boldsymbol{\sigma}} \cdot \mathbf{n} \, \mathrm{d}S \\ &= \overline{\boldsymbol{\sigma}} : \langle \boldsymbol{\epsilon}[\mathbf{u}] \rangle, \end{aligned} \tag{31}$$

from which it results (selecting $\mathbf{u}$ affine) that $\langle \boldsymbol{\sigma}^\dagger \rangle = \overline{\boldsymbol{\sigma}}$. Gathering the above results, we find that

$$\langle \boldsymbol{\sigma}^\dagger : \mathbf{e} + (\boldsymbol{\sigma}^\dagger \otimes \nabla) \therefore \boldsymbol{\phi} \rangle = \langle \boldsymbol{\sigma}^\dagger \rangle : \langle \mathbf{e} \rangle \tag{32}$$

and uniform stress boundary conditions ensure that the Hill–Mandel lemma holds.

Remark 4. *The uniform stress boundary conditions introduced above can be viewed as a generalization of the classical static uniform boundary conditions (Kanit et al., 2003). However, as already argued in section 2, while prescribing the traction at the boundary is indeed a static boundary condition, prescribing the remainder of the stress tensor involves the higher-order constitutive law of the material. We will therefore prefer the terminology "uniform stress boundary conditions" over "static uniform boundary conditions" in the present paper.*

Remark 5. *Alternative types of boundary conditions, that all ensure that the Hill–Mandel lemma holds, are proposed in Appendix C.*

4.2. Apparent compliance – Uniform stress boundary conditions

In the present section, we define the apparent stiffness of the SVE Ω from the following local problem

$$\begin{aligned} &\boldsymbol{\sigma} \cdot \nabla = \mathbf{0}, && \mathbf{e} = \mathbf{S} : \boldsymbol{\sigma}, && \text{(33a)} \\ &\mathbf{e} = \boldsymbol{\epsilon}[\mathbf{u}] + \boldsymbol{\phi} \cdot \nabla, && \boldsymbol{\phi} = \mathbf{M} \therefore (\boldsymbol{\sigma} \otimes \nabla), && \text{(33b)} \\ &\boldsymbol{\sigma}|_{\partial\Omega} = \overline{\boldsymbol{\sigma}}, && && \text{(33c)} \end{aligned}$$

where $\overline{\boldsymbol{\sigma}} \in \mathcal{T}_2$ is the constant prescribed stress at the boundary. It can be seen as the loading parameter for problem (33).

For this local problem, the stress tensor $\boldsymbol{\sigma}$ is divergence-free; its gradient is therefore trace-free, and $\mathbf{R} = \boldsymbol{\sigma} \otimes \nabla$, which allows to replace $\mathbf{R}$ with $\boldsymbol{\sigma} \otimes \nabla$ in equation $(15)_2$ [see equation $(33b)_2$ above]. Furthermore, the decomposition (9) of the tensor $\boldsymbol{\psi}$ has been introduced in the above problem. Equation $(33b)_1$ [which reproduces equation (10)] shows in particular that $\mathbf{e} - \boldsymbol{\phi} \cdot \nabla$ must be geometrically compatible.

The local problem (33) must of course be complemented with the continuity requirements (11) at each interface between two phases.

Sab et al. (2016) have recently shown that the boundary-value problem (33) is well-posed. Since this problem is linear, all local fields depend linearly on the loading parameter $\overline{\boldsymbol{\sigma}}$, which has been shown in section 4.1 to coincide with the macroscopic stress $\langle \boldsymbol{\sigma} \rangle$. We therefore introduce the apparent compliance $\mathbf{S}^\sigma(\Omega)$ as the fourth-rank tensor that maps the loading parameter onto the macroscopic strain

$$\langle \mathbf{e} \rangle = \mathbf{S}^\sigma(\Omega) : \overline{\boldsymbol{\sigma}} = \mathbf{S}^\sigma(\Omega) : \langle \boldsymbol{\sigma} \rangle. \tag{34}$$

Since the Hill–Mandel lemma holds for the uniform stress boundary conditions (33c), the apparent compliance $\mathbf{S}^\sigma(\Omega)$ is a symmetric, fourth-rank tensor. Besides, under the assumption of statistical homogeneity and ergodicity, it converges to the effective compliance $\mathbf{S}^{\text{eff}}$ as the size of the SVE Ω grows to infinity (Sab, 1992).

It can readily be verified that the solution to the local problem (33) minimizes the complementary strain energy W^* defined by equation (7). More precisely,

$$\begin{aligned} \overline{\boldsymbol{\sigma}} : \mathbf{S}^\sigma(\Omega) : \overline{\boldsymbol{\sigma}} = \inf \Big\{ &\langle \boldsymbol{\sigma} : \mathbf{S} : \boldsymbol{\sigma} + (\boldsymbol{\sigma} \otimes \nabla) \therefore \mathbf{M} \therefore (\boldsymbol{\sigma} \otimes \nabla) \rangle, \\ &\boldsymbol{\sigma} \in \mathcal{T}_2, \boldsymbol{\sigma} \cdot \nabla = \mathbf{0}, \boldsymbol{\sigma}|_{\partial\Omega} = \overline{\boldsymbol{\sigma}} \Big\}. \end{aligned} \tag{35}$$

In particular, using $\boldsymbol{\sigma}(\mathbf{x}) = \overline{\boldsymbol{\sigma}} = \text{const.}$ as test function, the classical Reuss bound is readily retrieved

$$\mathbf{S}^{\sigma}(\Omega) \leq \langle \mathbf{S} \rangle. \tag{36}$$

Quite remarkably, the above bound does not involve the local generalized compliance $\mathbf{M}$ of the material. The variational definition (35) of the apparent compliance also leads to the following inequality [this is a straightforward extension of the proof of Huet (1990)].

$$\mathbf{S}^{\text{eff}} \leq \mathbf{S}^{\sigma}(\Omega) \leq \langle \mathbf{S} \rangle. \tag{37}$$

4.3. Softening size-effect in stress-gradient materials

The definitions and properties introduced above allow us to prove that stress-gradient elasticity tends to soften heterogeneous materials, in a sense that will be made more precise below. By contrast, strain-gradient elasticity tends to stiffen heterogeneous materials (see e.g. Ma and Gao, 2014). This is proof enough that the stress- and strain- gradient theories define two different material models, and are not two dual formulations of the same material model as intuition might suggest. This result can be stated more precisely as follows. We consider two heterogeneous stress-gradient materials with compliances $\mathbf{S}^{\text{I}}$ and $\mathbf{S}^{\text{II}}$ and generalized compliances $\mathbf{M}^{\text{I}}$ and $\mathbf{M}^{\text{II}}$. We assume that material I is stiffer than material II: $\mathbf{S}^{\text{I}} \leq \mathbf{S}^{\text{II}}$ and $\mathbf{M}^{\text{I}} \leq \mathbf{M}^{\text{II}}$ everywhere in Ω (in the sense of quadratic forms).

Then, it results from the variational definition of apparent stiffness with uniform stress boundary conditions [see equation (35)] that the effective material I is stiffer than the effective material II: $\mathbf{S}^{\text{eff,I}} \leq \mathbf{S}^{\text{eff,II}}$.

Indeed, let $\boldsymbol{\sigma}^{\text{II}}$ be the solution to the local problem (33) for material II. Then, from equation (35), we first find for the apparent compliance of material I

$$\overline{\boldsymbol{\sigma}} : \mathbf{S}^{\sigma,\text{I}}(\Omega) : \overline{\boldsymbol{\sigma}} \leq \langle \boldsymbol{\sigma}^{\text{II}} : \mathbf{S}^{\text{I}} : \boldsymbol{\sigma}^{\text{II}} + \mathbf{R}^{\text{II}} \therefore \mathbf{M}^{\text{I}} \therefore \mathbf{R}^{\text{II}} \rangle. \tag{38}$$

where $\mathbf{R}^{\text{II}} = \mathbf{I}'_6 \therefore (\boldsymbol{\sigma}^{\text{II}} \otimes \nabla)$. Then, owing to the fact that material II is more compliant than material I

$$\overline{\boldsymbol{\sigma}} : \mathbf{S}^{\sigma,\text{I}}(\Omega) : \overline{\boldsymbol{\sigma}} \leq \langle \boldsymbol{\sigma}^{\text{II}} : \mathbf{S}^{\text{II}} : \boldsymbol{\sigma}^{\text{II}} + \mathbf{R}^{\text{II}} \therefore \mathbf{M}^{\text{II}} \therefore \mathbf{R}^{\text{II}} \rangle, \tag{39}$$

and the right-hand side quantity is equal to $\overline{\boldsymbol{\sigma}} : \mathbf{S}^{\sigma,\text{II}}(\Omega) : \overline{\boldsymbol{\sigma}}$. Letting the size of the SVE Ω grow to infinity then delivers $\mathbf{S}^{\text{eff,I}} \leq \mathbf{S}^{\text{eff,II}}$. It is noted that this result still holds if $\mathbf{M}^{\text{I}} = \mathbf{0}$ (no stress-gradient effects in material I). Besides, in the limit of large SVEs that is considered here, the actual boundary conditions are inconsequential (since the Hill–Mandel lemma guarantees their equivalence).

For the model with one material internal length defined in section 3 [see equation (20)], the above result means that increasing the material internal length (the size of the heterogeneities being unchanged) tends to decrease the effective stiffness. Conversely, decreasing the size of the heterogeneities (the material internal length being unchanged) tends to decrease the effective stiffness. In other words, stress-gradient materials exhibit as expected size-effects.

Strain-gradient models are often invoked to account for size-effects in nanocomposites. This is relevant for most nanocomposites, where so-called "positive" (or stiffening) size-effects are usually observed. However, numerical evidence from atomistic simulations suggest that some nanoparticles/polymer composites (Odegard et al., 2005; Davydov et al., 2014) might exhibit "negative" (softening) size-effects. For such materials, strain-gradient models are inadequate, while stress-gradient have the required qualitative behavior. It is emphasized that for both strain- and stress-gradient materials, boundary layers arise at the interface between matrix and inclusions (see section 5); such models are therefore conceptually suitable to describe interface effects in nanocomposites.

It should be noted that the one-dimensional differential model of Eringen (1983) is also known to exhibit softening size-effects (Reddy, 2007). More recently, Polizzotto (2014) and Challamel et al. (2016b) observed the same trend for beams (seen as prismatic solids) and lattices, respectively.

5. Eshelby's spherical inhomogeneity problem

In this section, we derive the dilute stress concentration tensor $\mathbf{B}^{\infty}$ of a spherical inhomogeneity. This tensor is the basic building block that will be required in section 6 for the derivation of Mori–Tanaka estimates of the effective properties of stress-gradient composites. It is computed by means of the solution to Eshelby's inhomogeneity problem (Eshelby, 1957). The general problem is stated in section 5.1; then, two analytical solutions are proposed in sections 5.2 and 5.3. The resulting dilute stress concentration tensor is finally derived and analyzed in section 5.4.

5.1. Statement of the problem

We consider a spherical inhomogeneity Ω_{i} centered at the origin of the unbounded, 3 dimensional space $\mathbb{R}^3$; a denotes the radius of the inhomogeneity (see Figure 1, left). Spherical coordinates r, θ, φ will be used in sections 5.2 and 5.3 below (see Figure 1, right) and it will be convenient to introduce the following second-rank tensors

$$\mathbf{p} = \mathbf{e}_r \otimes \mathbf{e}_r, \quad \text{and} \quad \mathbf{q} = \mathbf{e}_\theta \otimes \mathbf{e}_\theta + \mathbf{e}_\varphi \otimes \mathbf{e}_\varphi. \tag{40}$$

Both inhomogenity Ω_{i} and matrix Ω_{m} are made of linearly elastic stress-gradient materials: $\mathbf{S}_{\text{i}}$ (resp. $\mathbf{S}_{\text{m}}$) denotes the stiffness of the inhomogeneity (resp. the matrix). Similarly, $\mathbf{M}_{\text{i}}$ (resp. $\mathbf{M}_{\text{m}}$) denotes the generalized stiffness of the inhomogeneity (resp. the matrix). We use the simplified model introduced in section 3

$$\mathbf{M}_{\alpha} = \frac{\ell_{\alpha}^2}{2\mu}\left(\frac{1-2\nu_{\alpha}}{1+\nu_{\alpha}}\mathbf{J}_6 + \mathbf{K}_6\right), \tag{41}$$

where ℓ_{α} is the material internal length ($\alpha = \text{i}, \text{m}$). Introducing the indicator functions χ_{i} and χ_{m} of the inhomogeneity and matrix, respectively, we then define the heterogeneous compliance $\mathbf{S}$ and generalized compliance $\mathbf{M}$

$$\mathbf{S} = \chi_{\text{i}}\mathbf{S}_{\text{i}} + \chi_{\text{m}}\mathbf{S}_{\text{m}} \quad \text{and} \quad \mathbf{M} = \chi_{\text{i}}\mathbf{M}_{\text{i}} + \chi_{\text{m}}\mathbf{M}_{\text{m}}. \tag{42}$$

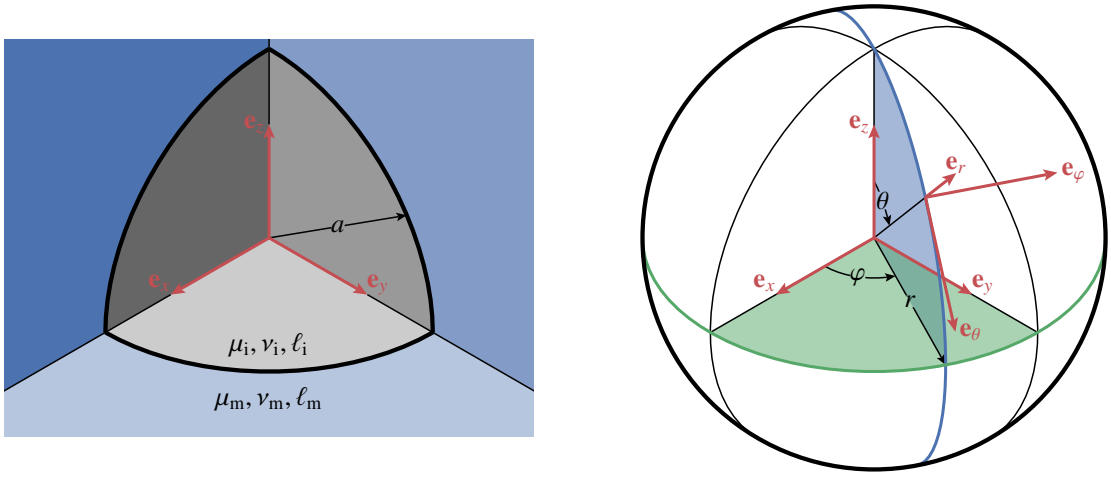

Figure 1: Eshelby's spherical inhomogeneity problem. *Left:* a spherical inhomogeneity embedded in an infinite matrix. *Right:* the spherical coordinates used in sections 5.2 and 5.3.

The spherical inhomogeneity is subjected to a uniform stress $\boldsymbol{\sigma}^\infty$ at infinity. The equations of the problem are the field equations (33), the continuity conditions (11) at the interface $r = a$ (with $\mathbf{n} = \mathbf{e}_r$) and the boundary condition $\lim_{r\to+\infty} \boldsymbol{\sigma} = \boldsymbol{\sigma}^\infty$.

The above problem is solved for two specific choices of the loading $\boldsymbol{\sigma}^\infty$ at infinity. In section 5.2, we derive the solution for an isotropic loading $\boldsymbol{\sigma}^\infty = \sigma^\infty \mathbf{I}_2$. The solution for a uniaxial loading $\boldsymbol{\sigma}^\infty = \sigma^\infty \mathbf{e}_z \otimes \mathbf{e}_z$ is then presented in section 5.3. In both cases, the derivation follows the same steps that are gathered below.

1. Postulate (divergence-free) stress tensor $\boldsymbol{\sigma}$.
2. Compute (trace-free) stress-gradient $\boldsymbol{\sigma} \otimes \nabla$.
3. Compute total strain $\mathbf{e}$ from equation $(33a)_2$.
4. Compute micro-displacement $\boldsymbol{\phi}$ from equation $(33b)_2$.
5. Express geometric compatibility of $\mathbf{e} - \boldsymbol{\phi} \cdot \nabla$ [see equation $(33b)_1$].
6. Use continuity conditions (11) and boundary conditions at infinity to compute integration constants.

To close this introductory section, it should be observed that the isotropic load case (see section 5.2) is not strictly necessary for the derivation of the dilute stress concentration tensor. Indeed, the uniaxial load case (see section 5.3) suffices to derive both spherical and deviatoric parts of this tensor (see section 5.4). Still, we chose to present the derivation of this simple solution, as an introduction to the more complex, uniaxial case.

5.2. *Isotropic loading at infinity*

In this section, we consider the case where the loading at infinity is isotropic, $\boldsymbol{\sigma}^\infty = \sigma^\infty \mathbf{I}_2$, and postulate the following divergence-free stress tensor

$$\boldsymbol{\sigma} = \sigma^\infty [f(r)\, \mathbf{I}_2 + \tfrac{1}{2} r f'(r)\, \mathbf{q}], \tag{43}$$

where f denotes a dimensionless, scalar function of r and f' its derivative with respect to r. It can readily be verified that [see equation (D.2) in Appendix D.1]

$$\mathbf{R} = \boldsymbol{\sigma} \otimes \nabla = \sigma^\infty [\tfrac{1}{2}(r f'' - f')\mathbf{q} \otimes \mathbf{e}_r + f' \mathbf{a}], \tag{44}$$

where the third-rank tensor $\mathbf{a}$ is defined as follows

$$\begin{aligned} \mathbf{a} = {} & 2\mathbf{q} \otimes \mathbf{e}_r + \mathbf{e}_r \otimes \mathbf{e}_r \otimes \mathbf{e}_r - \mathbf{sym}(\mathbf{e}_r \otimes \mathbf{e}_\theta) \otimes \mathbf{e}_\theta \\ & - \mathbf{sym}(\mathbf{e}_r \otimes \mathbf{e}_\varphi) \otimes \mathbf{e}_\varphi. \end{aligned} \tag{45}$$

Then, from equations $(33a)_2$ and $(33b)_2$ we find

$$\frac{2\mu}{\sigma^\infty} \mathbf{e} = \frac{\nu r f' + (1 - 2\nu) f}{1 + \nu} \mathbf{I}_2 + \tfrac{r}{2} f' \mathbf{q}, \tag{46a}$$

$$\frac{4\mu}{\ell^2 \sigma^\infty} \boldsymbol{\phi} = (r f'' - f') \mathbf{q} \otimes \mathbf{e}_r + \frac{2(1-\nu) f' - \nu r f''}{1 + \nu} \mathbf{a}, \tag{46b}$$

where the indices "i" and "m" have been omitted. It should be noted that equation (D.3) in Appendix D.1 has been used to derive equation (46b). Equation (D.4) in Appendix D.1 is then used to evaluate the divergence of equation (46b)

$$\begin{aligned} \frac{4\mu r (1+\nu)}{\ell^2 \sigma^\infty} \boldsymbol{\phi} \cdot \nabla = {} & [\nu r^2 f''' + (2 - 7\nu) r f'' + 8(1-\nu) f'] \mathbf{I}_2 \\ & + (r^2 f''' + 4 r f'' - 4 f') \mathbf{q}, \end{aligned} \tag{47}$$

and express that $\mathbf{e} - \boldsymbol{\phi} \cdot \nabla = \boldsymbol{\epsilon}[\mathbf{u}]$ is geometrically compatible [see equation $(33b)_1$]. To do so, it is observed that

$$\mathbf{e} - \boldsymbol{\phi} \cdot \nabla = \varepsilon_1(r)\, \mathbf{I}_2 + \varepsilon_2(r)\, \mathbf{q}, \tag{48}$$

so that the general compatibility conditions in spherical coordinates reduce to a unique scalar equation $\varepsilon_1 = [r(\varepsilon_1 + \varepsilon_2)]'$. Furthermore, the displacement is given by $\mathbf{u} = r(\varepsilon_1 + \varepsilon_2)\mathbf{e}_r$. We therefore get the following equation for f

$$\ell^2 (r^3 f^{(4)} + 8 r^2 f''' + 8 r f'' - 8 f') - (r^3 f'' + 4 r^2 f') = 0, \tag{49}$$

which admits four linearly independent solutions

$$1, \quad \frac{\ell^3}{r^3} \quad \text{and} \quad \left(\frac{\ell^3}{r^3} \mp \frac{\ell^2}{r^2} \right) \exp(\pm r/\ell). \tag{50}$$

Recalling that $\boldsymbol{\sigma}$ remains finite as $r \to 0$ and that $\lim_{r\to+\infty} \boldsymbol{\sigma} = \sigma^\infty \mathbf{I}_2$, it is finally found that

$$f(r) = \begin{cases} 1 + A_2 \rho_\mathrm{m}^3 \alpha_\mathrm{m}^{-3} + A_4 \rho_\mathrm{m}^2 (1 + \rho_\mathrm{m}) \mathfrak{E}_\mathrm{m} & (r > a), \\ B_1 + B_3 \rho_\mathrm{i}^2 (\rho_\mathrm{i} \mathfrak{S}_\mathrm{i} - \mathfrak{C}_\mathrm{i}) & (r < a), \end{cases} \tag{51}$$

where we have introduced $\alpha_\mathrm{m} = \ell_\mathrm{m}/a$, $\rho_\mathrm{m} = \ell_\mathrm{m}/r$, $\alpha_\mathrm{i} = \ell_\mathrm{i}/a$, $\rho_\mathrm{i} = \ell_\mathrm{i}/r$ and

$$\mathfrak{E}_\mathrm{m} = \exp[(a-r)/\ell_\mathrm{m}], \tag{52a}$$
$$\mathfrak{C}_\mathrm{i} = \exp(-a/\ell_\mathrm{i})\cosh(r/\ell_\mathrm{i}), \tag{52b}$$
$$\mathfrak{S}_\mathrm{i} = \exp(-a/\ell_\mathrm{i})\sinh(r/\ell_\mathrm{i}). \tag{52c}$$

In equation (51), the integration constants A_2, A_4, B_1 and B_3 are found from the continuity of the following scalar quantities at the interface $r = a$

$$\sigma_{rr}, \quad \sigma_{\theta\theta} = \sigma_{\varphi\varphi}, \quad \phi_{rrr} + u_r \quad \text{and} \quad \phi_{\theta\theta r} = \phi_{\varphi\varphi r}, \tag{53}$$

leading to four linearly independent equations. The closed-form expression of this system or its solution is too large to be reported here. As an illustration, we consider in Figure 2 the case of a stiff inhomogeneity

$$\mu_\mathrm{i} = 10\mu_\mathrm{m}, \quad \nu_\mathrm{i} = \nu_\mathrm{m} = 0.25, \tag{54}$$

and we study the influence of the material internal lengths ℓ_i and ℓ_m on the solution.

Figure 2 (left) shows the radial stress σ_{rr} for various combinations of $(\ell_\mathrm{i}, \ell_\mathrm{m})$. The classical case ($\ell_\mathrm{i} = \ell_\mathrm{m} = 0$) is also represented. From these plots, it is readily deduced that Eshelby's theorem (Eshelby, 1957) does not hold for stress-gradient elasticity. In other words, the stress is not uniform within the inhomogeneity. Indeed, the continuity condition $(11)_2$ induces a boundary layer at the matrix–inhomogeneity interface. The thickness of this boundary layer is about a few ℓ_i within the inhomogeneity [see equation (51)]. As a consequence, the stress field is nearly uniform at the core of the inhomogeneity for small values of the material internal length ℓ_i. Similarly, for small values of the material internal length ℓ_m of the matrix, the non-uniform stress within the inhomogeneity is close to the classical value.

Closer inspection of Figure 2 (left) shows that at a given point within the inhomogeneity, the radial stress does not evolve monotonically with the inhomogeneity's material internal length ℓ_i. This is better illustrated on Figure 2 (right), which shows the radial stress at the center of the inhomogeneity as a function of ℓ_i, for various values of ℓ_m. It is observed that the radial stress at the center reaches a maximum for a finite value of ℓ_i, which increases as ℓ_m increases.

5.3. *Uniaxial loading at infinity*

In this section, we consider the case of a uniaxial loading at infinity, $\boldsymbol{\sigma}^\infty = \sigma^\infty \mathbf{e}_z \otimes \mathbf{e}_z$. The derivation is significantly more involved than in the previous case; it is only briefly outlined here. We postulate the following stress tensor

$$\begin{aligned}\frac{\boldsymbol{\sigma}}{\sigma^\infty} &= [f_1(r)\cos^2\theta + f_2(r)\sin^2\theta]\mathbf{p} \\ &\quad + [f_3(r)\cos^2\theta + f_4(r)\sin^2\theta]\mathbf{q} \\ &\quad + f_5(r)\cos\theta\,\mathbf{sym}(\mathbf{e}_r \otimes \mathbf{e}_z) + f_6(r)\,\mathbf{e}_z \otimes \mathbf{e}_z.\end{aligned} \tag{55}$$

where $f_1, \ldots, f_6$ are unknown functions which depend on the radial variable r only. Expressing that the above-defined stress tensor must be divergence-free leads to the following differential equations

$$f_2 - f_3 - \tfrac{1}{2}f_5 + r\,(\tfrac{1}{2}f_2' - \tfrac{1}{4}f_5' - \tfrac{1}{2}f_6') = 0, \tag{56a}$$
$$f_2 - f_4 + \tfrac{1}{4}f_5 + \tfrac{1}{2}rf_2' = 0, \tag{56b}$$
$$f_1 - f_2 + f_5 + r(\tfrac{1}{2}f_1' - \tfrac{1}{2}f_2' + \tfrac{3}{4}f_5' + f_6') = 0, \tag{56c}$$

where primes again stand for derivation with respect to r. Computing the (trace-free) stress-gradient $\boldsymbol{\sigma} \otimes \nabla$, then the micro-displacement $\boldsymbol{\phi}$ and the strain $\mathbf{e}$ from the constitutive laws leads after simple but tedious algebra to the following decomposition of $\mathbf{e} - \boldsymbol{\phi} \cdot \nabla$

$$\begin{aligned}\mathbf{e} - \boldsymbol{\phi} \cdot \nabla &= [g_1(r)\cos^2\theta + g_2(r)\sin^2\theta]\mathbf{p} \\ &\quad + [g_3(r)\cos^2\theta + g_4(r)\sin^2\theta]\mathbf{q} \\ &\quad + g_5(r)\cos\theta\,\mathbf{sym}(\mathbf{e}_r \otimes \mathbf{e}_z) + g_6(r)\,\mathbf{e}_z \otimes \mathbf{e}_z,\end{aligned} \tag{57}$$

where $g_1, \ldots, g_6$ are linear combinations of the unknown functions $f_1, \ldots, f_6$ and their derivatives with respect to r (the actual relationships between $g_1, \ldots, g_6$ and $f_1, \ldots, f_6$ are too long to be reported here). Expressing that $\mathbf{e} - \boldsymbol{\phi} \cdot \nabla$ must be compatible [see equation $(33b)_1$] results in the following set of differential equations

$$g_1 = -\tfrac{1}{2}g_5 + r(g_4' + \tfrac{1}{2}g_5') - \tfrac{1}{2}r^2 g_6'', \tag{58a}$$
$$g_2 = g_4 + rg_4', \tag{58b}$$
$$g_3 = g_4 + \tfrac{1}{2}g_5 - \tfrac{1}{2}rg_6'. \tag{58c}$$

Gathering equations (56) and (58) finally leads to a linear system of six differential equations with $f_1, \ldots, f_6$ as unknowns. The general form of these functions is given in Appendix D.2, where twelve integration constants are identified. Enforcing the continuity conditions (11) at the interface $r = a$ (with $\mathbf{n} = \mathbf{e}_r$) again results in a linear system, the solution of which gives the values of these constants. Again, the closed-form expression of the linear system and its solution is too long to be reported here.

The axial stress σ_{zz} along the polar axis of the inhomogeneity is plotted for various combinations of $(\ell_\mathrm{i}, \ell_\mathrm{m})$ in Figure 3. The classical elastic constants of matrix and inhomogeneity are specified by equation (54). The plots are comparable to those of the isotropic load case (see Figure 2). A stress boundary layer is again observed at the matrix–inhomogeneity interface; it is induced by the stress continuity condition $(11)_2$. The axial stress at the center of the inclusion is not a monotonic function of the inhomogeneity's material length ℓ_i: it reaches a maximum for a finite value of ℓ_i, which increases as ℓ_m increases (the exact location of this maximum differs from the isotropic load case).

5.4. *The dilute stress concentration tensor of spherical inhomogeneities*

It is observed that Eshelby's inhomogeneity problem is linear. As such, the solution depends linearly on the loading parameter $\boldsymbol{\sigma}^\infty$. In particular, the average stress over the inhomogeneity is related to $\boldsymbol{\sigma}^\infty$ through the fourth-rank tensor $\mathbf{B}^\infty$

$$\frac{1}{V_\mathrm{i}}\int_{\Omega_\mathrm{i}} \boldsymbol{\sigma}\,\mathrm{d}V = \mathbf{B}^\infty : \boldsymbol{\sigma}^\infty \quad \text{with} \quad V_\mathrm{i} = \tfrac{4}{3}\pi a^3. \tag{59}$$

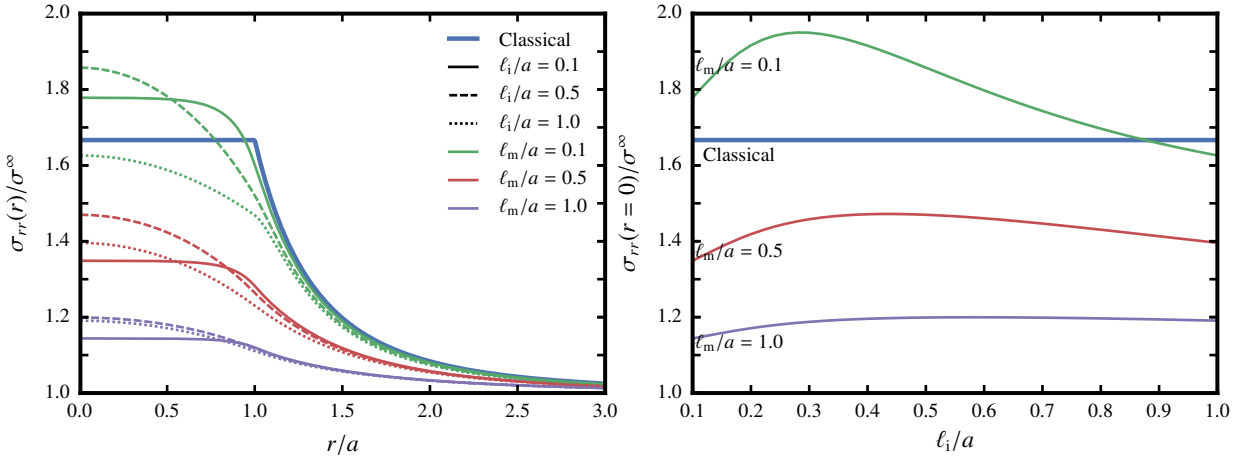

Figure 2: Solution to Eshelby's spherical inhomogeneity problem (isotropic loading at infinity). *Left:* plot of the radial stress σ_{rr} as a function of the distance to the center of the inhomogeneity, r. Line types (solid, dashed, dotted) correspond to various values of the material internal length ℓ_i of the inhomogeneity. *Right:* plot of the radial stress $\sigma_{rr}(r = 0)$ at the center of the inhomogeneity as a function of the inhomogeneity's material internal length ℓ_i. For both graphs, colors correspond to various values of the material internal length ℓ_m of the matrix. The thick line corresponds to the classical solution ($\ell_i = \ell_m = 0$).

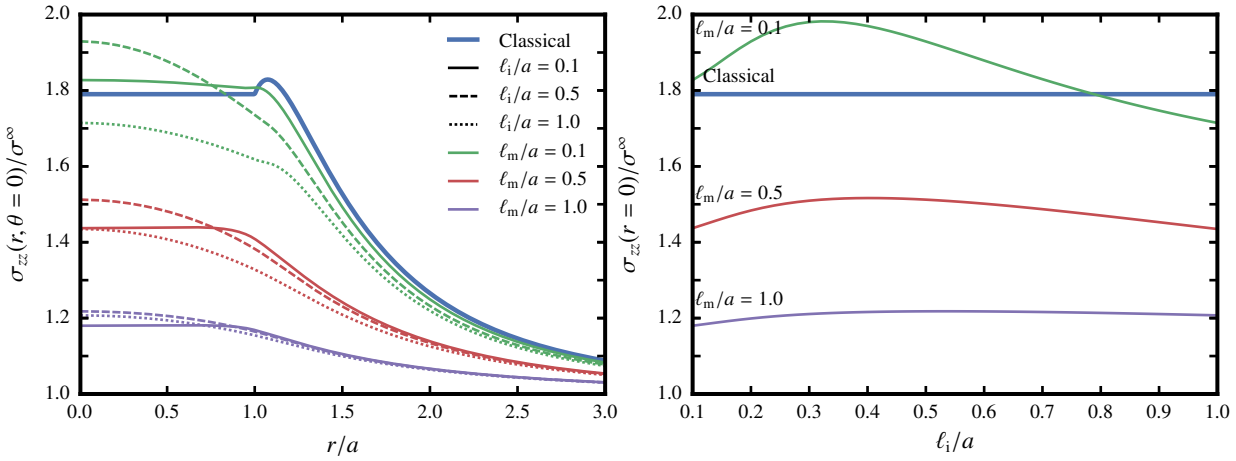

Figure 3: Solution to Eshelby's spherical inhomogeneity problem (uniaxial loading at infinity). *Left:* plot of the axial stress σ_{zz} along the polar axis ($\theta = 0$) as a function of the distance to the center of the inhomogeneity, r. Line types (solid, dashed, dotted) correspond to various values of the material internal length ℓ_i of the inhomogeneity. *Right:* plot of the axial stress $\sigma_{zz}(r = 0)$ at the center of the inhomogeneity as a function of the inhomogeneity's material internal length ℓ_i. For both graphs, colors correspond to various values of the material internal length ℓ_m of the matrix. The thick line corresponds to the classical solution ($\ell_i = \ell_m = 0$).

$\mathbf{B}^\infty$ is the so-called dilute stress concentration tensor of the spherical inhomogeneity. It can readily be computed from the solutions derived in section 5.3. Indeed, it is inferred from the symmetries of the problem under consideration that $\mathbf{B}^\infty$ is isotropic and can be decomposed as follows

$$\mathbf{B}^\infty = (\mathrm{sph}\,\mathbf{B}^\infty)\mathbf{J}_4 + (\mathrm{dev}\,\mathbf{B}^\infty)\mathbf{K}_4, \tag{60}$$

where $\mathbf{J}_4$ and $\mathbf{K}_4$ denote the classical fourth-rank spherical and deviatoric projection tensors, respectively, while $\mathrm{sph}\,\mathbf{B}^\infty$ and $\mathrm{dev}\,\mathbf{B}^\infty$ denote the (scalar) spherical and deviatoric part of the fourth-rank tensor $\mathbf{B}^\infty$

$$\mathrm{sph}\,\mathbf{B}^\infty = \mathbf{J}_4 :: \mathbf{B}^\infty \quad \text{and} \quad \mathrm{dev}\,\mathbf{B}^\infty = \tfrac{1}{5}\mathbf{K}_4 :: \mathbf{B}^\infty. \tag{61}$$

Indeed, using the general expression (55) of the stress tensor $\boldsymbol{\sigma}$ for the uniaxial load case (see section 5.3), it is readily found that the average stress over the inhomogeneity reads

$$\frac{15}{\sigma^\infty V_\mathrm{i}}\int_{\Omega_\mathrm{i}} \boldsymbol{\sigma}\,\mathrm{d}V = [2\,(F_1 - F_2 - F_3 + F_4) + 5F_5 + 15F_6]\,\mathbf{e}_z \otimes \mathbf{e}_z + (F_1 + 4F_2 + 4F_3 + 6F_4)\mathbf{I}_2, \tag{62}$$

$$\text{with} \quad F_k = \frac{3}{a^3}\int_0^a r^2 f_k(r)\,\mathrm{d}r \quad (k = 1, \ldots, 6). \tag{63}$$

From the decomposition (60) of the stress concentration tensor

$$\mathbf{B}^\infty : \mathbf{e}_z \otimes \mathbf{e}_z = \mathrm{dev}\,\mathbf{B}^\infty\ \mathbf{e}_z \otimes \mathbf{e}_z + \tfrac{1}{3}(\mathrm{sph}\,\mathbf{B}^\infty - \mathrm{dev}\,\mathbf{B}^\infty)\mathbf{I}_2, \tag{64}$$

which, upon combination with (62), finally gives

$$\mathrm{sph}\,\mathbf{B}^\infty = \tfrac{1}{3}(F_1 + F_5) + \tfrac{2}{3}(F_2 + F_3) + \tfrac{4}{3}F_4 + F_6, \tag{65a}$$

$$\mathrm{dev}\,\mathbf{B}^\infty = \tfrac{2}{15}(F_1 - F_2 - F_3 + F_4) + \tfrac{1}{3}F_5 + F_6. \tag{65b}$$

The above expressions of $\mathrm{sph}\,\mathbf{B}^\infty$ and $\mathrm{dev}\,\mathbf{B}^\infty$ are plotted in Figure 4 for various values of the material internal lengths ℓ_i and ℓ_m and the elastic constants specified by equation (54). It is observed that these coefficients tend to be generally more sensitive to the material internal length of the matrix, ℓ_m than to the material internal length of the inhomogeneity, ℓ_i.

6. Mori–Tanaka estimates of the effective properties of stress-gradient composites

In this section, the above solution to Eshelby's spherical inhomogeneity problem (see section 5) is used to derive Mori and Tanaka (1973) estimates of the effective bulk and shear moduli of stress-gradient composites with monodisperse, spherical inclusions. We adopt a stress-based approach (in which the primary outcome is the effective compliance), and extend the presentation of Benveniste (1987) to stress-gradient materials.

We use the same notations as in section 5. In particular, a denotes the common radius of all inclusions. Both matrix and inclusions are stress-gradient materials, with bulk (resp. shear) modulus κ_α (resp. μ_α) and material internal length ℓ_α ($\alpha = \mathrm{i}, \mathrm{m}$). Finally, f denotes the volume fraction of inclusions.

It can then readily be shown that the classical expressions of the Mori and Tanaka (1973) estimates of the effective properties remain valid for stress-gradient materials, provided that the classical dilute stress concentration tensor is substituted with the generalized dilute stress concentration tensor $\mathbf{B}^\infty$ derived in section 5.4. Therefore, using equation (14b) in Benveniste (1987)

$$\mathbf{S}_\mathrm{eff} = \mathbf{S}_\mathrm{m} + f(\mathbf{S}_\mathrm{i} - \mathbf{S}_\mathrm{m}) : \mathbf{B}^\infty : [(1 - f)\mathbf{I}_4 + f\mathbf{B}^\infty]^{-1}. \tag{66}$$

The above expression is readily split into its spherical and deviatoric parts. Inversion then gives the estimates of the effective bulk and shear moduli. It should be noted that unlike the studies of Sharma and Dasgupta (2002), Zhang and Sharma (2005) and Ma and Gao (2014) for strain-gradient materials, our estimates are based on the solution to Eshelby's inhomogeneity (not inclusion) problem. We therefore do not need to rely on an approximate equivalent inclusion assumption to derive the above Mori–Tanaka estimates.

As an illustration, the resulting effective moduli are plotted in Figure 5 as a function of the volume fraction f of inclusions. We again chose the classical moduli of both phases according to equation (54), while we assumed that $\ell_\mathrm{i} = \ell_\mathrm{m}$ (since it was shown in section 5.4 that the dilute stress tensor is not very sensitive to ℓ_i).

As expected, it is observed that for small values of the material internal length, the proposed estimates are close to the classical Mori and Tanaka (1973) estimates. Conversely, for larger values of the material internal length, these estimates tend to the classical bound of Reuss. This was also expected, since large material internal lengths tend to favor phase-wise constant stress fields (as already argued at the end of section 3). It should however be noted that the limit as $\ell_\mathrm{i}, \ell_\mathrm{m} \to +\infty$ is purely formal. Indeed, the above analysis is carried out within the framework of the scale separation hypothesis (23) considered in section 4; as a consequence, the largest material internal length considered in Figure 5 is $\ell_\mathrm{i} = \ell_\mathrm{m} = a$.

Figure 5 also shows the Mori–Tanaka estimates of the effective elastic properties of strain-gradient materials proposed by Ma and Gao (2014). These estimates are based on the so-called simplified strain gradient elasticity theory initially proposed by Altan and Aifantis (1992, 1997) and developed by Gao and Park (2007). It is recalled that our own simplified material model (described in section 3) is very close in spirit to that of Gao and Park (2007), which makes the comparison in Figure 5 relevant.

Figure 5 is a visual illustration of the essential differences between strain- and stress-gradient materials that were already pointed out in section 4.3. Indeed, the region comprised between the Reuss and Voigt bounds is clearly divided in two non-overlapping subregions. Strain-gradient materials systematically fall in the region comprised between the classical effective properties and the corresponding upper-bounds of Voigt (stiffening size-effect), while stress-gradient materials systematically fall in the region comprised between the classical effective properties and the corresponding lower-bounds of Reuss (softening size-effect). This again shows that, although conceptually similar (one might be tempted to say that they are "dual"),

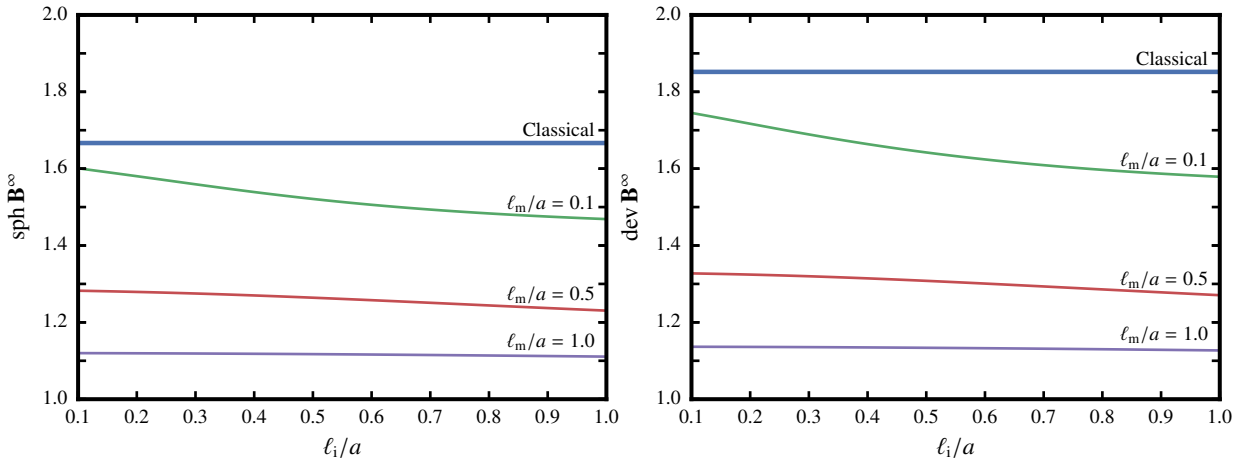

Figure 4: The spherical (*left*) and deviatoric (*right*) parts of the dilute stress concentration tensor $\mathbf{B}^\infty$ as a function of the inhomogeneity's material internal length ℓ_i. Like the previous graphs, colors correspond to various values of the material internal length ℓ_m of the matrix. The thick line corresponds to the classical solution ($\ell_i = \ell_m = 0$).

the strain- and stress-gradient models define widely different materials.

7. Conclusion

In this paper, we investigated the homogenization of stress-gradient composites. We adopted the material model introduced by Forest and Sab (2012) and analyzed mathematically by Sab et al. (2016).

We first proposed a simplified model of stress-gradient, linear elasticity. Like the model of Altan and Aifantis (1992, 1997) and Gao and Park (2007) for strain-gradient elasticity, it requires only *one* (rather than three in the general, isotropic case) material internal length.

Homogenization of stress-gradient materials was then carried out under the assumption that the material internal length is at most of the same order as the typical size of the heterogeneities. Observing that such materials are expected to behave macroscopically as classical linearly elastic materials, we proposed a general homogenization framework. We introduced uniform stress boundary conditions that fulfill the macro-homogeneity condition and proposed variational definitions of the effective elastic properties. We concluded that stress-gradient materials exhibit a softening size-effect. More precisely, a decrease of the size of the heterogeneities (the material internal length being kept constant) induces a decrease of the macroscopic stiffness. This result shows that stress-gradient materials are not equivalent to strain-gradient materials (which exhibit the opposite effect).

The paper closes with an illustration of the above general results. We produced Mori–Tanaka estimates of the effective properties of stress-gradient composites with spherical inclusions. These estimates are based on the solution to Eshelby's spherical inhomogeneity problem that is also derived here. More advanced homogenization techniques (including Hashin–Shtrikman bounds and full field simulations) will be explored in future works.

Our stress-gradient model is suitable to materials that exhibit softening size-effects. To the best of our knowledge, such materials are yet to be identified experimentally, even if they have been evidenced by atomistic simulations. The present work could then provide sound modelling grounds for this kind of materials.

8. Acknowledgements

This work has benefited from a French government grant managed by ANR within the frame of the national program Investments for the Future ANR-11-LABX-022-01.

Appendix A. Trace-free part of a third-rank tensor

It is recalled that the sixth-rank tensor $\mathbf{I}'_6$ is defined as the orthogonal projection (in the sense of the "$\therefore$" scalar product) onto the subspace $\mathcal{T}'_3$ of trace-free, third-rank tensors. Being a projector, $\mathbf{I}'_6$ enjoys the classical property $\mathbf{I}'_6 \therefore \mathbf{I}'_6 = \mathbf{I}'_6$.

The remainder of this section is devoted to the derivation of a closed-form expression for $\mathbf{I}'_6$. For any vector $\mathbf{v}$, it is first observed that $\mathbf{I}_4 \cdot \mathbf{v} \in \mathcal{T}_3$ is orthogonal to $\mathcal{T}'_3$. Indeed, it is readily verified [using equation (3b)] that for all $\mathbf{T} \in \mathcal{T}_3$, $\mathbf{T} \therefore \mathbf{I}_4 = \mathbf{T} : \mathbf{I}_2$. Therefore, for all $\mathbf{R} \in \mathcal{T}'_3$

$$(\mathbf{I}_4 \cdot \mathbf{v}) \therefore \mathbf{R} = \mathbf{R} \therefore \mathbf{I}_4 \cdot \mathbf{v} = \mathbf{v} \cdot \mathbf{R} : \mathbf{I}_2 = 0, \tag{A.1}$$

where the last equality results from the fact that $\mathbf{R}$ is trace-free. By a similar line of reasoning, we find the trace of the third-rank tensor $\mathbf{I}_4 \cdot \mathbf{v}$

$$(\mathbf{I}_4 \cdot \mathbf{v}) : \mathbf{I}_2 = \frac{d+1}{2}\mathbf{v}, \tag{A.2}$$

where d denotes the dimension of the physical space. We now consider $\mathbf{T} \in \mathcal{T}_3$, and introduce the third-rank tensor $\mathbf{Q}$

$$\mathbf{Q} = \frac{2}{d+1}\mathbf{I}_4 \cdot (\mathbf{T} : \mathbf{I}_2). \tag{A.3}$$

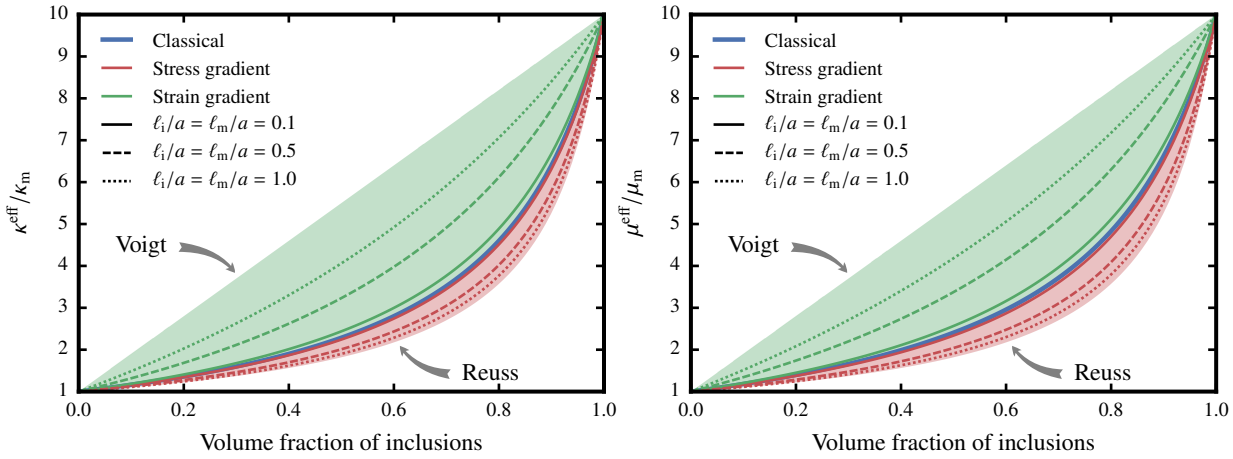

Figure 5: Mori–Tanaka estimates of the effective bulk (*left*) and shear (*right*) moduli of the composite κ^{eff} and μ^{eff}, as a function of the volume fraction of inclusions, f. The estimates are represented for both stress- and strain-gradient materials.

From equation (A.2), we find that $\mathbf{T}$ and $\mathbf{Q}$ have same trace; thus, $\mathbf{R} = \mathbf{T} - \mathbf{Q}$ is trace-free. Furthermore, $\mathbf{Q} \therefore \mathbf{R} = 0$, since $\mathbf{Q}$ is of the form $\mathbf{I}_2 \cdot \mathbf{v}$. In other words, we have produced the orthogonal decomposition $\mathbf{T} = \mathbf{Q} + \mathbf{R}$, where $\mathbf{R}$ is trace-free. Therefore, $\mathbf{R} = \mathbf{I}'_6 \therefore \mathbf{T}$ and

$$\mathbf{I}'_6 \therefore \mathbf{T} = \mathbf{T} - \frac{2}{d+1}\mathbf{I}_4 \cdot (\mathbf{T} : \mathbf{I}_2). \tag{A.4}$$

In particular, for a stress field $\boldsymbol{\sigma}$ statically admissible with the body forces $\mathbf{b}$ ($\boldsymbol{\sigma} \cdot \nabla + \mathbf{b} = \mathbf{0}$)

$$\begin{aligned}\boldsymbol{\sigma} \otimes \nabla &= \mathbf{R} + \tfrac{1}{2}\mathbf{I}_4 \cdot (\boldsymbol{\sigma} \otimes \nabla) : \mathbf{I}_2 = \mathbf{R} + \tfrac{1}{2}\mathbf{I}_4 \cdot (\boldsymbol{\sigma} \cdot \nabla) \\ &= \mathbf{R} - \tfrac{1}{2}\mathbf{I}_4 \cdot \mathbf{b},\end{aligned} \tag{A.5}$$

where $\mathbf{R} = \mathbf{I}'_6 \therefore (\boldsymbol{\sigma} \otimes \nabla)$ and $d = 3$.

Appendix B. Isotropic stress-gradient linear elasticity

In order to show that the constitutive law of linearly elastic, isotropic stress-gradient materials is defined by five material parameters, the generalized compliance $\mathbf{M}$ is first expanded in the basis of sixth-rank, isotropic tensors $\mathbf{T}^{\text{I}}, \ldots, \mathbf{T}^{\text{VI}}$ introduced by Monchiet and Bonnet (2010)

$$T^{\text{I}}_{ijkpqr} = \delta_{ij}\delta_{pq}\delta_{kr}, \qquad T^{\text{IV}}_{ijkpqr} = I_{pqkr}\delta_{ij}, \tag{B.1a}$$
$$T^{\text{II}}_{ijkpqr} = I_{ijpq}\delta_{kr}, \qquad T^{\text{V}}_{ijkpqr} = \text{sym}_{pq}(I_{ijpr}\delta_{kq}), \tag{B.1b}$$
$$T^{\text{III}}_{ijkpqr} = I_{ijkr}\delta_{pq}, \qquad T^{\text{VI}}_{ijkpqr} = \text{sym}_{ij}(I_{pqir}\delta_{jk}), \tag{B.1c}$$

where the components I_{ijkl} of the fourth-rank identity tensor $\mathbf{I}_4$ are given by equation (3b) and "sym_{ij}" denotes symmetrization with respect to the indices i and j. It can readily be verified that

$$\mathbf{I}_6 = \mathbf{T}^{\text{II}} \quad \text{and} \quad \mathbf{I}'_6 = \mathbf{T}^{\text{II}} - \tfrac{1}{2}\mathbf{T}^{\text{VI}}. \tag{B.2}$$

Keeping in mind that $\mathbf{M}$ must have the major symmetry (which requires the coefficients of $\mathbf{T}^{\text{III}}$ and $\mathbf{T}^{\text{IV}}$ to be equal), the following expansion of $\mathbf{M}$ is adopted

$$\mathbf{M} = m_{\text{I}}\mathbf{T}^{\text{I}} + m_{\text{II}}\mathbf{T}^{\text{II}} + m_{\text{III}}(\mathbf{T}^{\text{III}} + \mathbf{T}^{\text{IV}}) + m_{\text{V}}\mathbf{T}^{\text{V}} + m_{\text{VI}}\mathbf{T}^{\text{VI}}. \tag{B.3}$$

$\therefore$	$\mathbf{J}_6$	$\mathbf{K}_6$	$\mathbf{H}_6$
$\mathbf{J}_6$	$\mathbf{J}_6$	$\mathbf{0}$	$\mathbf{0}$
$\mathbf{K}_6$	$\mathbf{0}$	$\mathbf{K}_6$	$\mathbf{H}_6$
$\mathbf{H}_6$	$\mathbf{0}$	$\mathbf{H}_6$	$\mathbf{H}_6$

Table B.1: Multiplication table for the tensors $\mathbf{J}_6$, $\mathbf{K}_6$ and $\mathbf{H}_6$.

The coefficients $m_{\text{I}}, m_{\text{II}}, m_{\text{III}}, m_{\text{V}}$ and m_{VI} of this decomposition are not independent, since identity (14) must be satisfied. Using the decomposition $(\text{B.2})_2$ of the projector $\mathbf{I}'_6$ and the multiplication table of the $\mathbf{T}^{\bullet}$ for the triple dot product $\therefore$ [see Table 1 in Monchiet and Bonnet (2010)], the following relations are found

$$\begin{aligned}&\mathbf{I}'_6 \therefore \mathbf{T}^{\text{I}} \therefore \mathbf{I}'_6 = \mathbf{T}^{\text{I}} - \tfrac{1}{2}(\mathbf{T}^{\text{III}} + \mathbf{T}^{\text{IV}}) + \tfrac{1}{4}\mathbf{T}^{\text{VI}}, \\ &\mathbf{I}'_6 \therefore \mathbf{T}^{\text{II}} \therefore \mathbf{I}'_6 = \mathbf{I}'_6 = \mathbf{T}^{\text{II}} - \tfrac{1}{2}\mathbf{T}^{\text{VI}}, \\ &\mathbf{I}'_6 \therefore \mathbf{T}^{\text{V}} \therefore \mathbf{I}'_6 = -\tfrac{1}{4}(\mathbf{T}^{\text{III}} + \mathbf{T}^{\text{IV}}) + \mathbf{T}^{\text{V}} - \tfrac{1}{8}\mathbf{T}^{\text{VI}}, \\ &\mathbf{I}'_6 \therefore \mathbf{T}^{\text{III}} \therefore \mathbf{I}'_6 = \mathbf{I}'_6 \therefore \mathbf{T}^{\text{IV}} \therefore \mathbf{I}'_6 = \mathbf{I}'_6 \therefore \mathbf{T}^{\text{VI}} \therefore \mathbf{I}'_6 = \mathbf{0}.\end{aligned} \tag{B.4}$$

Clearly, the first three tensors are linearly independent, which shows that the dimension of the space of sixth-rank, isotropic tensors $\mathbf{M}$ with major symmetry and such that $\mathbf{I}'_6 \therefore \mathbf{M} \therefore \mathbf{I}'_6$ is 3. The tensors $\mathbf{J}_6$, $\mathbf{K}_6$ and $\mathbf{H}_6$

$$\begin{aligned}\mathbf{J}_6 &= \tfrac{2}{5}\mathbf{T}^{\text{I}} - \tfrac{1}{5}(\mathbf{T}^{\text{III}} + \mathbf{T}^{\text{IV}}) + \tfrac{1}{10}\mathbf{T}^{\text{VI}}, \\ \mathbf{K}_6 &= -\tfrac{2}{5}\mathbf{T}^{\text{I}} + \mathbf{T}^{\text{II}} + \tfrac{1}{5}(\mathbf{T}^{\text{III}} + \mathbf{T}^{\text{IV}}) - \tfrac{3}{5}\mathbf{T}^{\text{VI}}, \\ \mathbf{H}_6 &= -\tfrac{1}{15}\mathbf{T}^{\text{I}} + \tfrac{1}{3}\mathbf{T}^{\text{II}} - \tfrac{2}{15}(\mathbf{T}^{\text{III}} + \mathbf{T}^{\text{IV}}) + \tfrac{2}{3}\mathbf{T}^{\text{V}} - \tfrac{4}{15}\mathbf{T}^{\text{VI}}\end{aligned} \tag{B.5}$$

define a basis for this space, and it is readily verified that $\mathbf{J}_6 + \mathbf{K}_6 = \mathbf{I}'_6$. The multiplication table for this basis is provided in table B.1.

The above analysis shows that the compliance $\mathbf{S}$ and generalized compliance $\mathbf{M}$ of isotropic, linearly elastic stress-gradient materials are therefore defined by *five* material parameters μ (shear modulus), ν (Poisson ratio), ℓ_J, ℓ_K and ℓ_H (material internal lengths)

$$2\mu\,\mathbf{S} = \tfrac{1-2\nu}{1+\nu}\mathbf{J}_4 + \mathbf{K}_4 \quad \text{and} \quad 2\mu\,\mathbf{M} = \ell_J^2\mathbf{J}_6 + \ell_K^2\mathbf{K}_6 + \ell_H^2\mathbf{H}_6. \tag{B.6}$$

Appendix C. Alternative boundary conditions that are consistent with the Hill–Mandel lemma

In the present appendix, we propose alternative boundary conditions for the local problem of homogenization that ensure that the resulting stresses and strains satisfy the Hill–Mandel lemma.

Consistency with the Hill–Mandel lemma is checked through the verification of equation (27).

Appendix C.1. Kinematic uniform boundary conditions (KUBC)

We assume here that $\boldsymbol{\psi}\cdot\mathbf{n} = \mathbf{sym}[(\bar{\mathbf{e}}\cdot\mathbf{x})\otimes\mathbf{n}]$, where $\bar{\mathbf{e}}$ is a constant tensor (generalized uniform kinematic boundary conditions). Then

$$\begin{aligned}\frac{1}{V}\int_{\partial\Omega}\boldsymbol{\sigma}^\dagger : \boldsymbol{\psi}\cdot\mathbf{n}\,\mathrm{d}S &= \frac{1}{V}\int_{\partial\Omega}\mathbf{x}\cdot\bar{\mathbf{e}}\cdot\boldsymbol{\sigma}^\dagger\cdot\mathbf{n}\,\mathrm{d}S\\ &= \frac{1}{V}\int_{\Omega}(\mathbf{x}\cdot\bar{\mathbf{e}}\cdot\boldsymbol{\sigma}^\dagger)\cdot\nabla\,\mathrm{d}V\\ &= \frac{1}{V}\int_{\Omega}\boldsymbol{\sigma}^\dagger : \bar{\mathbf{e}}\,\mathrm{d}V = \langle\boldsymbol{\sigma}^\dagger\rangle : \bar{\mathbf{e}},\end{aligned} \tag{C.1}$$

where the fact that $\boldsymbol{\sigma}^\dagger$ is divergence-free has been used. Substituting $\boldsymbol{\sigma}^\dagger = \text{const.}$ in the above also delivers [with equation (28)]

$$\langle\mathbf{e}\rangle = \frac{1}{V}\int_{\partial\Omega}\boldsymbol{\psi}\cdot\mathbf{n}\,\mathrm{d}S = \bar{\mathbf{e}}. \tag{C.2}$$

Combining equations (C.1) and (C.2), it is finally found that the Hill–Mandel lemma holds for the proposed boundary conditions, since

$$\frac{1}{V}\int_{\partial\Omega}\boldsymbol{\sigma}^\dagger : \boldsymbol{\psi}\cdot\mathbf{n}\,\mathrm{d}S = \langle\boldsymbol{\sigma}^\dagger\rangle : \langle\mathbf{e}\rangle. \tag{C.3}$$

The apparent compliance of the SVE Ω can therefore be defined from the solution to the following local problem [compare with problem (33)]

$$\boldsymbol{\sigma}\cdot\nabla = \mathbf{0}, \qquad \mathbf{e} = \mathbf{S} : \boldsymbol{\sigma}, \tag{C.4a}$$

$$\mathbf{e} = \boldsymbol{\epsilon}[\mathbf{u}] + \boldsymbol{\phi}\cdot\nabla, \qquad \boldsymbol{\phi} = \mathbf{M} \therefore (\boldsymbol{\sigma}\otimes\nabla), \tag{C.4b}$$

$$\boldsymbol{\psi}\cdot\mathbf{n}|_{\partial\Omega} = \mathbf{sym}[(\bar{\mathbf{e}}\cdot\mathbf{x})\otimes\mathbf{n}], \tag{C.4c}$$

where $\bar{\mathbf{e}}\in\mathcal{T}_2$ is the constant prescribed macroscopic strain; it is the loading parameter for the above problem.

The macroscopic stress $\langle\boldsymbol{\sigma}\rangle$ depends linearly on the loading parameter $\bar{\mathbf{e}}$. The apparent stiffness $\mathbf{C}^\varepsilon(\Omega)$ is defined as the linear operator which maps $\langle\mathbf{e}\rangle = \bar{\mathbf{e}}$ to $\langle\boldsymbol{\sigma}\rangle$: $\langle\boldsymbol{\sigma}\rangle = \mathbf{C}^\varepsilon(\Omega) : \bar{\mathbf{e}}$.

It is a symmetric, fourth-rank tensor which, under the assumption of statistical homogeneity and ergodicity, converges to the effective stiffness $\mathbf{C}^{\text{eff}}$ as the size of the SVE Ω grows to infinity (Sab, 1992).

It can readily be verified that the solution to the local problem (C.4) minimizes the strain energy W^* defined by equation (7). More precisely,

$$\begin{aligned}\bar{\mathbf{e}} : \mathbf{C}^\varepsilon(\Omega) : \bar{\mathbf{e}} = \inf\Big\{&\langle\boldsymbol{\epsilon}[\mathbf{u}] : \mathbf{C} : \boldsymbol{\epsilon}[\mathbf{u}] + \boldsymbol{\phi} \therefore \mathbf{L} \therefore \boldsymbol{\phi}\rangle,\\ &\boldsymbol{\psi}\in\mathcal{T}_3, \boldsymbol{\psi}\cdot\mathbf{n}|_{\partial\Omega} = \mathbf{sym}[(\bar{\mathbf{e}}\cdot\mathbf{x})\otimes\mathbf{n}],\\ &\mathbf{u} = \tfrac{1}{2}\boldsymbol{\psi} : \mathbf{I}_2, \boldsymbol{\phi} = \mathbf{I}'_6 \therefore \boldsymbol{\psi}\Big\}.\end{aligned} \tag{C.5}$$

In particular, using $\boldsymbol{\psi}(\mathbf{x}) = \mathbf{I}_4\cdot\bar{\mathbf{e}}\cdot\mathbf{x}$ as test function ($\mathbf{u} = \bar{\mathbf{e}}\cdot\mathbf{x}$ and $\boldsymbol{\phi} = \mathbf{0}$), the classical Voigt bound is readily retrieved

$$\mathbf{C}^\varepsilon(\Omega) \le \langle\mathbf{C}\rangle. \tag{C.6}$$

Again, the above bound does not involve the local generalized stiffness $\mathbf{L}$ of the material. By a straightforward extension of the work of Huet (1990), the variational definition (C.5) of the apparent stiffness also leads to the following inequality

$$\mathbf{C}^{\text{eff}} \le \mathbf{C}^\varepsilon(\Omega) \le \langle\mathbf{C}\rangle. \tag{C.7}$$

Appendix C.2. Periodic boundary conditions (PBC)

We now assume that the SVE Ω is a rectangular prism $\Omega = (0, L_1)\times\cdots\times(0, L_d)$ and that $\boldsymbol{\sigma}^\dagger$ is Ω-periodic while $\boldsymbol{\psi}'\cdot\mathbf{n}$ is Ω-skew-periodic, where $\bar{\mathbf{e}}$ is a constant tensor and $\boldsymbol{\psi}' = \boldsymbol{\psi} - \mathbf{I}_4\cdot\bar{\mathbf{e}}\cdot\mathbf{x}$.

It is first observed that, at the boundary of the unit-cell,

$$\boldsymbol{\psi}\cdot\mathbf{n} = \boldsymbol{\psi}'\cdot\mathbf{n} + \mathbf{sym}[(\bar{\mathbf{e}}\cdot\mathbf{x})\otimes\mathbf{n}], \tag{C.8}$$

and, using equation (C.1)

$$\frac{1}{V}\int_{\partial\Omega}\boldsymbol{\sigma}^\dagger : \boldsymbol{\psi}\cdot\mathbf{n}\,\mathrm{d}S = \frac{1}{V}\int_{\partial\Omega}\boldsymbol{\sigma}^\dagger : \boldsymbol{\psi}'\cdot\mathbf{n}\,\mathrm{d}S + \langle\boldsymbol{\sigma}^\dagger\rangle : \bar{\mathbf{e}}, \tag{C.9}$$

The first integral vanishes since $\boldsymbol{\sigma}^\dagger : \boldsymbol{\psi}'\cdot\mathbf{n}$ is Ω-skew-periodic

$$\frac{1}{V}\int_{\partial\Omega}\boldsymbol{\sigma}^\dagger : \boldsymbol{\psi}\cdot\mathbf{n}\,\mathrm{d}S = \langle\boldsymbol{\sigma}^\dagger\rangle : \bar{\mathbf{e}}, \tag{C.10}$$

and we find again [plugging $\boldsymbol{\sigma}^\dagger = \text{const.}$ in equation (C.10)] that $\bar{\mathbf{e}} = \langle\mathbf{e}\rangle$. We have therefore verified that equation (27), hence the Hill–Mandel lemma, hold for the periodic boundary conditions stated above.

Summing up, the apparent stiffness for periodic boundary conditions is defined from the solution to the following local problem [compare with problem (33)]

$$\boldsymbol{\sigma}\cdot\nabla = \mathbf{0}, \qquad \mathbf{e} = \mathbf{S} : \boldsymbol{\sigma}, \tag{C.11a}$$

$$\mathbf{e} = \boldsymbol{\epsilon}[\mathbf{u}] + \boldsymbol{\phi}\cdot\nabla, \qquad \boldsymbol{\phi} = \mathbf{M} \therefore (\boldsymbol{\sigma}\otimes\nabla), \tag{C.11b}$$

$$\boldsymbol{\sigma}\text{ is }\Omega\text{-periodic}, \qquad (\boldsymbol{\psi} - \mathbf{I}_4\cdot\bar{\mathbf{e}}\cdot\mathbf{x})\cdot\mathbf{n} \text{ is } \Omega\text{-skew-periodic}, \tag{C.11c}$$

where $\bar{\mathbf{e}}\in\mathcal{T}_2$ is the constant prescribed macroscopic strain; it is the loading parameter for the above problem.

Again, the macroscopic stress $\langle\boldsymbol{\sigma}\rangle$ depends linearly on the loading parameter $\bar{\mathbf{e}}$. The apparent stiffness $\mathbf{C}^{\text{per}}(\Omega)$ is defined as the symmetric linear operator which maps $\langle\mathbf{e}\rangle = \bar{\mathbf{e}}$ to $\langle\boldsymbol{\sigma}\rangle$: $\langle\boldsymbol{\sigma}\rangle = \mathbf{C}^{\text{per}}(\Omega) : \bar{\mathbf{e}}$.

Appendix C.3. Mixed boundary conditions

The mixed boundary conditions presented here can also be seen as an extension of the classical static uniform boundary conditions, where only the traction (not the full stress tensor) is prescribed at the boundary. We now assume that

$$\boldsymbol{\sigma}^\dagger\cdot\mathbf{n}|_{\partial\Omega} = \overline{\boldsymbol{\sigma}}\cdot\mathbf{n} \quad\text{and}\quad \mathbf{a}\cdot(\boldsymbol{\psi}\cdot\mathbf{n})\cdot\mathbf{a}|_{\partial\Omega} = \mathbf{0}, \tag{C.12}$$

where $\overline{\boldsymbol{\sigma}} \in \mathcal{T}_2$ is a constant, prescribed stress a $\mathbf{a} = \mathbf{I}_2 - \mathbf{n}\otimes\mathbf{n}$ is the projection onto the tangent plane to the boundary. Owing to the symmetry of $\boldsymbol{\sigma}$, $\mathbf{a}$ and $\boldsymbol{\psi}\cdot\mathbf{n}$, we then have at the boundary

$$\begin{aligned}(\boldsymbol{\sigma}^\dagger - \overline{\boldsymbol{\sigma}}) : \boldsymbol{\psi}\cdot\mathbf{n} &= [(\boldsymbol{\sigma}^\dagger - \overline{\boldsymbol{\sigma}})\cdot(\mathbf{a}+\mathbf{n}\otimes\mathbf{n})] : \boldsymbol{\psi}\cdot\mathbf{n} \\ &= (\boldsymbol{\sigma}^\dagger - \overline{\boldsymbol{\sigma}}) : (\mathbf{a}\cdot\boldsymbol{\psi}\cdot\mathbf{n}) \\ &\quad + [(\boldsymbol{\sigma}^\dagger\cdot\mathbf{n} - \overline{\boldsymbol{\sigma}}\cdot\mathbf{n})\otimes\mathbf{n}] : \boldsymbol{\psi}\cdot\mathbf{n}, \quad \text{(C.13)}\end{aligned}$$

and both terms vanish owing to boundary conditions $(\text{C.12})_1$ and $(\text{C.12})_2$, respectively. Therefore

$$\begin{aligned}\frac{1}{V}\int_{\partial\Omega}\boldsymbol{\sigma}^\dagger : \boldsymbol{\psi}\cdot\mathbf{n}\,\mathrm{d}S &= \frac{1}{V}\int_{\partial\Omega}\overline{\boldsymbol{\sigma}} : \boldsymbol{\psi}\cdot\mathbf{n}\,\mathrm{d}S \\ &= \overline{\boldsymbol{\sigma}} : \left(\frac{1}{V}\int_{\partial\Omega}\boldsymbol{\psi}\cdot\mathbf{n}\,\mathrm{d}S\right) = \overline{\boldsymbol{\sigma}} : \langle\mathbf{e}\rangle, \quad \text{(C.14)}\end{aligned}$$

where equation (28) has been used. Furthermore, it results from boundary condition $(\text{C.12})_1$ and the equilibrium equation $\boldsymbol{\sigma}^\dagger\cdot\nabla = \mathbf{0}$ that $\langle\boldsymbol{\sigma}^\dagger\rangle = \overline{\boldsymbol{\sigma}}$. As a conclusion, identity (27) is again verified, which ensures that the Hill–Mandel lemma holds.

The apparent compliance of the SVE Ω can therefore be defined from the solution to the following local problem [compare with problem (33)]

$$\begin{aligned}&\boldsymbol{\sigma}\cdot\nabla = \mathbf{0}, && \mathbf{e} = \mathbf{S} : \boldsymbol{\sigma}, && \text{(C.15a)}\\ &\mathbf{e} = \boldsymbol{\epsilon}[\mathbf{u}] + \boldsymbol{\phi}\cdot\nabla, && \boldsymbol{\phi} = \mathbf{M} \therefore (\boldsymbol{\sigma}\otimes\nabla), && \text{(C.15b)}\\ &\boldsymbol{\sigma}\cdot\mathbf{n}|_{\partial\Omega} = \overline{\boldsymbol{\sigma}}\cdot\mathbf{n}, && \mathbf{a}\cdot(\boldsymbol{\psi}\cdot\mathbf{n})\cdot\mathbf{a}|_{\partial\Omega} = \mathbf{0}, && \text{(C.15c)}\end{aligned}$$

where $\overline{\boldsymbol{\sigma}} \in \mathcal{T}_2$ is the constant prescribed macroscopic stress; it is the loading parameter for the above problem.

The macroscopic strain $\langle\mathbf{e}\rangle$ depends linearly on the loading parameter $\overline{\boldsymbol{\sigma}}$. The apparent compliance $\mathbf{S}^T(\Omega)$ (where T stands for "traction") is defined as the linear operator which maps $\langle\boldsymbol{\sigma}\rangle = \overline{\boldsymbol{\sigma}}$ to $\langle\mathbf{e}\rangle$: $\langle\mathbf{e}\rangle = \mathbf{S}^T(\Omega) : \overline{\boldsymbol{\sigma}}$.

Remark 6. *It should be noted that equation (C.15c) amounts to only 6 linearly independent scalar boundary conditions (as expected). Indeed, $\boldsymbol{\psi}\cdot\mathbf{n}$ is a second-rank, symmetric tensor, with only three independent in-plane components.*

Appendix D. On Eshelby's spherical inhomogeneity problem

Appendix D.1. Isotropic loading at infinity

In the present appendix, we gather some identities which prove useful for the derivation of the solution to Eshelby's problem of a spherical inhomogeneity subjected to isotropic loading at infinity (see section 5.2).

We start with the evaluation of the gradient of the stress tensor $\boldsymbol{\sigma}$ given by equation (43). From the identity $\mathbf{p} + \mathbf{q} = \mathbf{I}_2$ [see equation (40) for the definition of $\mathbf{p}$ and $\mathbf{q}$], we have

$$\mathbf{q}\otimes\nabla = -\mathbf{p}\otimes\nabla = -\partial_\theta\mathbf{p}\otimes\frac{\mathbf{e}_\theta}{r} - \partial_\varphi\mathbf{p}\otimes\frac{\mathbf{e}_\varphi}{r\sin\theta}, \quad \text{(D.1)}$$

which, upon substitution of the partial derivatives of $\mathbf{e}_r$ with respect to θ and φ, leads to

$$\mathbf{q}\otimes\nabla = -\frac{2}{r}[\mathbf{sym}(\mathbf{e}_r\otimes\mathbf{e}_\theta)\otimes\mathbf{e}_\theta + \mathbf{sym}(\mathbf{e}_r\otimes\mathbf{e}_\varphi)\otimes\mathbf{e}_\varphi], \quad \text{(D.2)}$$

and expression (44) readily follows. Then, simple algebra leads to the following identities, which are required to evaluate $\boldsymbol{\phi} = \mathbf{M} \therefore \mathbf{R}$ [see equation (46b)]

$$\mathbf{J}_6 \therefore \mathbf{a} = \mathbf{a}, \quad \mathbf{K}_6 \therefore \mathbf{a} = \mathbf{0} \quad \text{and} \quad \mathbf{H}_6 \therefore \mathbf{a} = \mathbf{0}, \quad \text{(D.3)}$$

where the sixth-rank tensors $\mathbf{J}_6$, $\mathbf{K}_6$ and $\mathbf{H}_6$ have been defined in Appendix A. Finally, proceeding with a similar technique as for $\mathbf{q}\otimes\nabla$, the following identities are readily derived

$$r[(\mathbf{q}\otimes\mathbf{e}_r)\cdot\nabla] = 2\mathbf{q} \quad \text{and} \quad r(\mathbf{a}\cdot\nabla) = 4\mathbf{I}_2 - \mathbf{q}, \quad \text{(D.4)}$$

which are then used to establish equation (47).

Appendix D.2. Uniaxial loading at infinity

In this case, the general expression (55) of the stress tensor depends on twelve integration constants. Recalling first that $\boldsymbol{\sigma} \to \sigma^\infty\mathbf{e}_z\otimes\mathbf{e}_z$ as $r \to +\infty$, it can be shown that the general solution reads, outside the spherical inhomogeneity ($r > a$)

$$\begin{aligned}f_1 = &-\frac{\rho_\mathrm{m}}{2}\mathfrak{E}_\mathrm{m}[(3\rho_\mathrm{m}^2 + 3\rho_\mathrm{m} + 1)C_4 \\ &+ \rho_\mathrm{m}(39\rho_\mathrm{m}^3 + 39\rho_\mathrm{m}^2 + 16\rho_\mathrm{m} + 3)C_{10} \\ &+ (39\rho_\mathrm{m}^4 + 39\rho_\mathrm{m}^3 + 9\rho_\mathrm{m}^2 - 4\rho_\mathrm{m} - 3)C_{11}] \\ &- \frac{2+\nu_\mathrm{m}}{2\nu_\mathrm{m}}\frac{\rho_\mathrm{m}^3}{\alpha_\mathrm{m}^3}C_2 + \frac{\rho_\mathrm{m}^3}{\alpha_\mathrm{m}^3}C_6 - \frac{13}{2}\frac{\rho_\mathrm{m}^5}{\alpha_\mathrm{m}^5}C_7, \quad \text{(D.5)}\end{aligned}$$

$$\begin{aligned}f_2 = &\rho_\mathrm{m}^2\mathfrak{E}_\mathrm{m}[\rho_\mathrm{m}(3\rho_\mathrm{m}^2 + 3\rho_\mathrm{m} + 1)C_{10} \\ &+ (3\rho_\mathrm{m}^3 + 3\rho_\mathrm{m}^2 - 1)C_{11}] + \frac{\rho_\mathrm{m}^3}{\alpha_\mathrm{m}^3}C_6 + \frac{\rho_\mathrm{m}^5}{\alpha_\mathrm{m}^5}C_7, \quad \text{(D.6)}\end{aligned}$$

$$\begin{aligned}f_3 = &\frac{\rho_\mathrm{m}}{4}\mathfrak{E}_\mathrm{m}[-(3\rho_\mathrm{m}^2 + 3\rho_\mathrm{m} + 1)C_4 \\ &+ (4\rho_\mathrm{m}^2 + 1)(3\rho_\mathrm{m}^2 + 3\rho_\mathrm{m} + 1)C_{10} \\ &+ 2(6\rho_\mathrm{m}^4 + 6\rho_\mathrm{m}^3 + 9\rho_\mathrm{m}^2 + 7\rho_\mathrm{m} + 3)C_{11}] \\ &+ \frac{1-\nu_\mathrm{m}}{4\nu_\mathrm{m}}\frac{\rho_\mathrm{m}^3}{\alpha_\mathrm{m}^3}C_2 - \frac{1}{2}\frac{\rho_\mathrm{m}^3}{\alpha_\mathrm{m}^3}C_6 + \frac{\rho_\mathrm{m}^5}{\alpha_\mathrm{m}^5}C_7, \quad \text{(D.7)}\end{aligned}$$

$$\begin{aligned}f_4 = &\frac{\rho_\mathrm{m}}{4}\mathfrak{E}_\mathrm{m}[(3\rho_\mathrm{m}^2 + 3\rho_\mathrm{m} + 1)C_4 \\ &- \rho_\mathrm{m}(3\rho_\mathrm{m}^3 + 3\rho_\mathrm{m}^2 + 2\rho_\mathrm{m} + 1)C_{10} \\ &- (3\rho_\mathrm{m}^4 + 3\rho_\mathrm{m}^3 + 9\rho_\mathrm{m}^2 + 8\rho_\mathrm{m} + 1)C_{11}] \\ &+ \frac{1}{4}\frac{\rho_\mathrm{m}^3}{\alpha_\mathrm{m}^3}C_2 - \frac{1}{2}\frac{\rho_\mathrm{m}^3}{\alpha_\mathrm{m}^3}C_6 - \frac{1}{4}\frac{\rho_\mathrm{m}^5}{\alpha_\mathrm{m}^5}C_7, \quad \text{(D.8)}\end{aligned}$$

$$\begin{aligned}f_5 = &\rho_\mathrm{m}\mathfrak{E}_\mathrm{m}[(3\rho_\mathrm{m}^2 + 3\rho_\mathrm{m} + 1)C_4 \\ &+ \rho_\mathrm{m}(15\rho_\mathrm{m}^3 + 15\rho_\mathrm{m}^2 + 6\rho_\mathrm{m} + 1)C_{10} \\ &+ (15\rho_\mathrm{m}^4 + 15\rho_\mathrm{m}^3 - 3\rho_\mathrm{m}^2 - 8\rho_\mathrm{m} - 3)C_{11}] \\ &+ \frac{\rho_\mathrm{m}^3}{\alpha_\mathrm{m}^3}C_2 + 5\frac{\rho_\mathrm{m}^5}{\alpha_\mathrm{m}^5}C_7, \quad \text{(D.9)}\end{aligned}$$

$$
\begin{aligned}
f_6 = & -\frac{\rho_\mathrm{m}}{2}\mathfrak{E}_\mathrm{m}[(2\rho_\mathrm{m}^2+2\rho_\mathrm{m}+1)C_4 \\
& +\rho_\mathrm{m}^2(3\rho_\mathrm{m}^2+3\rho_\mathrm{m}+1)C_{10} \\
& +(3\rho_\mathrm{m}^4+3\rho_\mathrm{m}^3-5\rho_\mathrm{m}^2-6\rho_\mathrm{m}-3)C_{11}] \\
& +1+\frac{1-2\nu_\mathrm{m}}{6\nu_\mathrm{m}}\frac{\rho_\mathrm{m}^3}{\alpha_\mathrm{m}^3}C_2-\frac{1}{2}\frac{\rho_\mathrm{m}^5}{\alpha_\mathrm{m}^5}C_7, \qquad \text{(D.10)}
\end{aligned}
$$

where $\alpha_\mathrm{m}, \rho_\mathrm{m}$ and $\mathfrak{E}_\mathrm{m}$ have been introduced in section 5.2, while C_2, C_4, C_6, C_7, C_{10} and C_{11} are integration constants.

Stresses must also remain finite at the center of the inhomogeneity ($r = 0$). This leads to the following form of the general solution, inside the inhomogeneity ($r < a$)

$$
\begin{aligned}
f_1 = & D_3[-\rho_\mathrm{i}(3\rho_\mathrm{i}^2+1)\mathfrak{S}_\mathrm{i}+3\rho_\mathrm{i}^2\mathfrak{C}_\mathrm{i}] \\
& +D_8[-\rho_\mathrm{i}^3(39\rho_\mathrm{i}^2+16)\mathfrak{S}_\mathrm{i}+3\rho_\mathrm{i}^2(13\rho_\mathrm{i}^2+1)\mathfrak{C}_\mathrm{i}] \\
& +D_9[3\rho_\mathrm{i}(-13\rho_\mathrm{i}^4-3\rho_\mathrm{i}^2+1)\mathfrak{S}_\mathrm{i}+\rho_\mathrm{i}^2(39\rho_\mathrm{i}^2-4)\mathfrak{C}_\mathrm{i}] \\
& +D_5+D_{12}\alpha_\mathrm{i}^2\Big(28-\frac{7+10\nu_\mathrm{i}}{\nu_\mathrm{i}}\rho_\mathrm{i}^{-2}\Big), \qquad \text{(D.11)}
\end{aligned}
$$

$$
\begin{aligned}
f_2 = & D_8[2\rho_\mathrm{i}^3(3\rho_\mathrm{i}^2+1)\mathfrak{S}_\mathrm{i}-6\rho_\mathrm{i}^4\mathfrak{C}_\mathrm{i}] \\
& +D_9[6\rho_\mathrm{i}^5\mathfrak{S}_\mathrm{i}-2\rho_\mathrm{i}^2(3\rho_\mathrm{i}^2-1)\mathfrak{C}_\mathrm{i}] \\
& +D_5+D_{12}\alpha_\mathrm{i}^2(28+\rho_\mathrm{i}^{-2}), \qquad \text{(D.12)}
\end{aligned}
$$

$$
\begin{aligned}
f_3 = & \tfrac{1}{2}D_3[-\rho_\mathrm{i}(3\rho_\mathrm{i}^2+1)\mathfrak{S}_\mathrm{i}+3\rho_\mathrm{i}^2\mathfrak{C}_\mathrm{i}] \\
& +\tfrac{1}{2}D_8[\rho_\mathrm{i}(12\rho_\mathrm{i}^4+7\rho_\mathrm{i}^2+1)\mathfrak{S}_\mathrm{i}-3\rho_\mathrm{i}^2(4\rho_\mathrm{i}^2+1)\mathfrak{C}_\mathrm{i}] \\
& +D_9[3\rho_\mathrm{i}(2\rho_\mathrm{i}^4+3\rho_\mathrm{i}^2+1)\mathfrak{S}_\mathrm{i}-\rho_\mathrm{i}^2(6\rho_\mathrm{i}^2+7)\mathfrak{C}_\mathrm{i}] \\
& +D_5+D_{12}\alpha_\mathrm{i}^2\Big(28-\frac{7+6\nu_\mathrm{i}}{\nu_\mathrm{i}}\rho_\mathrm{i}^{-2}\Big), \qquad \text{(D.13)}
\end{aligned}
$$

$$
\begin{aligned}
f_4 = & \tfrac{1}{2}D_3[\rho_\mathrm{i}(3\rho_\mathrm{i}^2+1)\mathfrak{S}_\mathrm{i}-3\rho_\mathrm{i}^2\mathfrak{C}_\mathrm{i}] \\
& +\tfrac{1}{2}D_8[-\rho_\mathrm{i}^3(3\rho_\mathrm{i}^2+2)\mathfrak{S}_\mathrm{i}+\rho_\mathrm{i}^2(3\rho_\mathrm{i}^2+1)\mathfrak{C}_\mathrm{i}] \\
& +\tfrac{1}{2}D_9[-\rho_\mathrm{i}(3\rho_\mathrm{i}^4+9\rho_\mathrm{i}^2+1)\mathfrak{S}_\mathrm{i}+\rho_\mathrm{i}^2(3\rho_\mathrm{i}^2+8)\mathfrak{C}_\mathrm{i}] \\
& +D_5+D_{12}\alpha_\mathrm{i}^2(28+5\rho_\mathrm{i}^{-2}), \qquad \text{(D.14)}
\end{aligned}
$$

$$
\begin{aligned}
f_5 = & D_3[2\rho_\mathrm{i}(3\rho_\mathrm{i}^2+1)\mathfrak{S}_\mathrm{i}-6\rho_\mathrm{i}^2\mathfrak{C}_\mathrm{i}] \\
& +D_8[6\rho_\mathrm{i}^3(5\rho_\mathrm{i}^2+2)\mathfrak{S}_\mathrm{i}-2\rho_\mathrm{i}^2(15\rho_\mathrm{i}^2+1)\mathfrak{C}_\mathrm{i}] \\
& +D_9[6\rho_\mathrm{i}(5\rho_\mathrm{i}^4-\rho_\mathrm{i}^2-1)\mathfrak{S}_\mathrm{i}-2\rho_\mathrm{i}^2(15\rho_\mathrm{i}^2-8)\mathfrak{C}_\mathrm{i}] \\
& +12\frac{\alpha_\mathrm{i}^2}{\rho_\mathrm{i}^2}D_{12}, \qquad \text{(D.15)}
\end{aligned}
$$

$$
\begin{aligned}
f_6 = & D_3[-\rho_\mathrm{i}(2\rho_\mathrm{i}^2+1)\mathfrak{S}_\mathrm{i}+2\rho_\mathrm{i}^2\mathfrak{C}_\mathrm{i}] \\
& +D_8[-\rho_\mathrm{i}^3(3\rho_\mathrm{i}^2+1)\mathfrak{S}_\mathrm{i}+3\rho_\mathrm{i}^4\mathfrak{C}_\mathrm{i}] \\
& +D_9[-\rho_\mathrm{i}(3\rho_\mathrm{i}^4-5\rho_\mathrm{i}^2-3)\mathfrak{S}_\mathrm{i}+3\rho_\mathrm{i}^2(\rho_\mathrm{i}^2-2)\mathfrak{C}_\mathrm{i}] \\
& +D_1+\frac{7-4\nu_\mathrm{i}}{\nu_\mathrm{i}}\frac{\alpha_\mathrm{i}^2}{\rho_\mathrm{i}^2}D_{12}, \qquad \text{(D.16)}
\end{aligned}
$$

where α_i, ρ_i, $\mathfrak{C}_\mathrm{i}$ and $\mathfrak{S}_\mathrm{i}$ have been introduced in section 5.2, while D_1, D_3, D_5, D_8, D_9 and D_{12} are integration constants. The twelve unknown integration constants are found by enforcing the continuity of $\boldsymbol{\sigma}$ and $\mathbf{sym}(\mathbf{u}\otimes\mathbf{e}_r)+\boldsymbol{\phi}\cdot\mathbf{e}_r$ at the interface $r = a$.

Altan, B., Aifantis, E., 1997. On some aspects in the special theory of gradient elasticity. Journal of the Mechanical Behavior of Materials 8 (3), 231–282.

Altan, S., Aifantis, E., 1992. On the structure of the mode III crack-tip in gradient elasticity. Scripta Metallurgica et Materialia 26 (2), 319–324.

Askes, H., Aifantis, E. C., 2011. Gradient elasticity in statics and dynamics: An overview of formulations, length scale identification procedures, finite element implementations and new results. International Journal of Solids and Structures 48 (13), 1962–1990.

Benveniste, Y., 1987. A new approach to the application of Mori-Tanaka's theory in composite materials. Mechanics of Materials 6 (2), 147–157.

Broese, C., Tsakmakis, C., Beskos, D., 2016. Mindlin's micro-structural and gradient elasticity theories and their thermodynamics. Journal of Elasticity, 1–46.

Challamel, N., Reddy, J., Wang, C., 2016a. Eringen's stress gradient model for bending of nonlocal beams. Journal of Engineering Mechanics 142 (12), 04016095.

Challamel, N., Wang, C. M., Elishakoff, I., 2016b. Nonlocal or gradient elasticity macroscopic models: A question of concentrated or distributed microstructure. Mechanics Research Communications 71, 25–31.

Cosserat, E., Cosserat, F., 1909. Théorie des corps déformables. A. Hermann et fils, Paris.

Davydov, D., Voyiatzis, E., Chatzigeorgiou, G., Liu, S., Steinmann, P., Böhm, M. C., Müller-Plathe, F., 2014. Size effects in a silica-polystyrene nanocomposite: Molecular dynamics and surface-enhanced continuum approaches. Soft Materials 12 (sup1), S142–S151.

Eringen, A. C., 1983. On differential equations of nonlocal elasticity and solutions of screw dislocation and surface waves. Journal of Applied Physics 54 (9), 4703–4710.

Eringen, A. C., 1999. Microcontinuum field theories. Vol. I. Foundations and Solids. Springer-Verlag New York, Inc.

Eringen, A. C., 2002. Nonlocal continuum field theories. Springer-Verlag New York, Inc.

Eshelby, J. D., 1957. The determination of the elastic field of an ellipsoidal inclusion, and related problems. Proceedings of the Royal Society of London. Series A, Mathematical and Physical Sciences 241 (1226), 376–396.

Forest, S., Aifantis, E. C., 2010. Some links between recent gradient thermo-elasto-plasticity theories and the thermomechanics of generalized continua. International Journal of Solids and Structures 47 (25–26), 3367–3376.

Forest, S., Pradel, F., Sab, K., 2001. Asymptotic analysis of heterogeneous cosserat media. International Journal of Solids and Structures 38 (26–27), 4585–4608.

Forest, S., Sab, K., 2012. Stress gradient continuum theory. Mechanics Research Communications 40, 16–25.

Forest, S., Sab, K., 2017. Finite-deformation second order micromorphic theory and its relations to strain and stress gradient models. Mathematics and Mechanics of SolidsAvailable online.

Gao, X.-L., Park, S., 2007. Variational formulation of a simplified strain gradient elasticity theory and its application to a pressurized thick-walled cylinder problem. International Journal of Solids and Structures 44 (22–23), 7486–7499.

Huet, C., 1990. Application of variational concepts to size effects in elastic heterogeneous bodies. Journal of the Mechanics and Physics of Solids 38 (6), 813–841.

Kanit, T., Forest, S., Galliet, I., Mounoury, V., Jeulin, D., 2003. Determination of the size of the representative volume element for random composites: statistical and numerical approach. International Journal of Solids and Structures 40 (13-14), 3647–3679.

Lebée, A., Sab, K., 2011. A bending-gradient model for thick plates. Part I: Theory. International Journal of Solids and Structures 48 (20), 2878–2888.

Lebée, A., Sab, K., 2017a. On the generalization of Reissner plate theory to laminated plates, part I: Theory. Journal of Elasticity 126 (1), 39–66.

Lebée, A., Sab, K., 2017b. On the generalization of Reissner plate theory to laminated plates, part II: Comparison with the bending-gradient theory. Journal of Elasticity 126 (1), 67–94.

Ma, H., Gao, X.-L., 2014. A new homogenization method based on a simplified

strain gradient elasticity theory. Acta Mechanica 225 (4-5), 1075–1091.
Marsden, J., Hughes, T. J. R., 1994. Mathematical foundations of elasticity. Dover Publications, Inc., New York.
Mindlin, R., 1965. Second gradient of strain and surface-tension in linear elasticity. International Journal of Solids and Structures 1 (4), 417 – 438.
Mindlin, R., Eshel, N., 1968. On first strain-gradient theories in linear elasticity. International Journal of Solids and Structures 4 (1), 109–124.
Mindlin, R. D., 1964. Micro-structure in linear elasticity. Archive for Rational Mechanics and Analysis 16 (1), 51–78.
Monchiet, V., Bonnet, G., 2010. Inversion of higher order isotropic tensors with minor symmetries and solution of higher order heterogeneity problems. Proceedings of the Royal Society of London A: Mathematical, Physical and Engineering Sciences 467 (2126).
Mori, T., Tanaka, K., 1973. Average stress in matrix and average elastic energy of materials with misfitting inclusions. Acta Metallurgica 21 (5), 571–574.
Mühlhaus, H. B., Vardoulakis, I., 1987. The thickness of shear bands in granular materials. Géotechnique 37 (3), 271–283.
Odegard, G., Clancy, T., Gates, T., 2005. Modeling of the mechanical properties of nanoparticle/polymer composites. Polymer 46 (2), 553–562.
Ostoja-Starzewski, M., 2006. Material spatial randomness: From statistical to representative volume element. Probabilistic Engineering Mechanics 21 (2), 112–132.
Polizzotto, C., 2014. Stress gradient versus strain gradient constitutive models within elasticity. International Journal of Solids and Structures 51 (9), 1809–1818.
Polizzotto, C., 2016. Variational formulations and extra boundary conditions within stress gradient elasticity theory with extensions to beam and plate models. International Journal of Solids and Structures 80, 405–419.
Reddy, J., 2007. Nonlocal theories for bending, buckling and vibration of beams. International Journal of Engineering Science 45 (2), 288–307.
Sab, K., 1992. On the homogenization and the simulation of random materials. European Journal of Mechanics - A/Solids 11 (5), 585–607.
Sab, K., Legoll, F., Forest, S., 2016. Stress gradient elasticity theory: Existence and uniqueness of solution. Journal of Elasticity 123 (2), 179–201.
Sharma, P., Dasgupta, A., 2002. Average elastic fields and scale-dependent overall properties of heterogeneous micropolar materials containing spherical and cylindrical inhomogeneities. Physical Review B 66, 224110.
Timoshenko, S., 1921. On the correction for shear of the differential equation for transverse vibrations of prismatic bars. The London, Edinburgh, and Dublin Philosophical Magazine and Journal of Science 41 (245), 744–746.
Zhang, X., Sharma, P., 2005. Inclusions and inhomogeneities in strain gradient elasticity with couple stresses and related problems. International Journal of Solids and Structures 42 (13), 3833–3851.
Zhou, S., Li, A., Wang, B., 2016. A reformulation of constitutive relations in the strain gradient elasticity theory for isotropic materials. International Journal of Solids and Structures 80, 28–37.